The Yang Research Group
Precise Synthesis Lab at Tongji University

Group Topic

Neidig group work

Reporter: Dong-Song Zheng

Date: 2025.06.20

CONTENTS
目录

Michael L. Neidig

Professional experience

2022 - present Professor, University of Oxford;

2011 - 2021 Professor, University of Rochester;

2007 - 2011 Senior Research Chemist, Dow Chemical; Postdoc, Los Alamos National Lab (洛斯·阿拉莫斯国家实验室担任主任博士后研究员).

2002 - 2007 Ph.D., Stanford University; Advisor: Prof. Edward Solomon;

1999 - 2002 M.Phil., University of Cambridge;

1995 - 1999 B.S., Colgate University;

Research

(1) Iron-Catalysed Transformations for Sustainable Catalysis in Organic Synthesis.

(2) C-H Activation with Earth-Abundant Metals.

(3) Electronic Structure and Spectroscopy in Inorganic, Bioinorganic and Materials Chemistry.

(4) Bonding and Reactivity Studies in Molecular f-Element Chemistry.

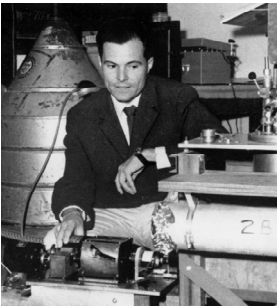

Rudolf L. MÖSSBAUER

1958: discovers the "Mössbauer effect".
1961: receives the Nobel Prize.

穆斯堡尔效应：γ-射线的无反冲共振吸收的现象。

共振吸收

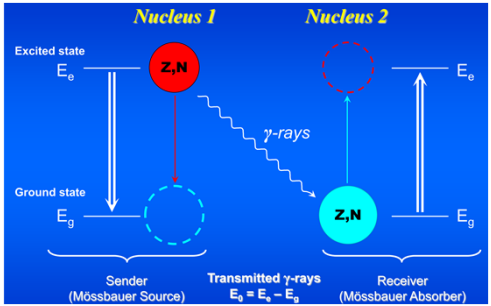

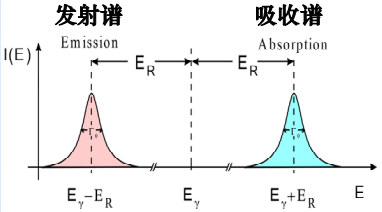

无反冲共振吸收

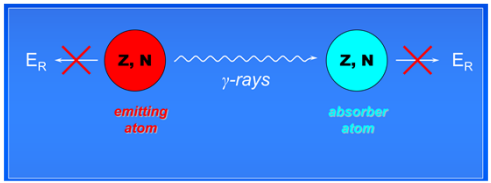

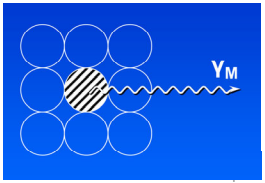

经典理论：无反冲共振吸收也需要多普勒运动补偿能量差

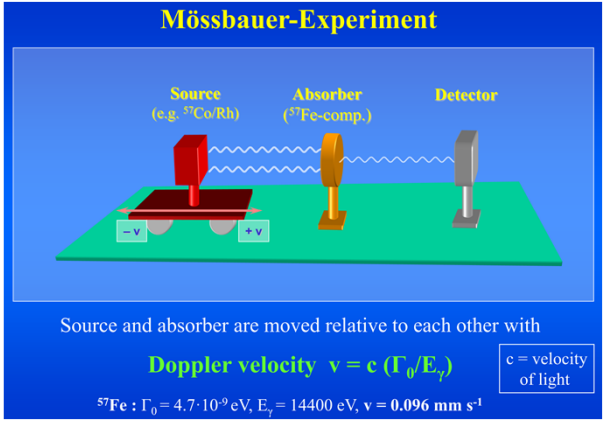

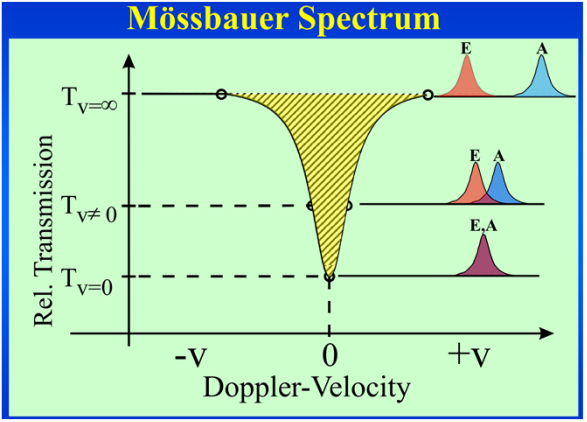

多普勒效应：当波源相对于观察者运动时，观察者收到的波的频率将发生变化。

当发射源相对吸收体运动时，吸收体吸收的伽马射线的能量将发生变化。

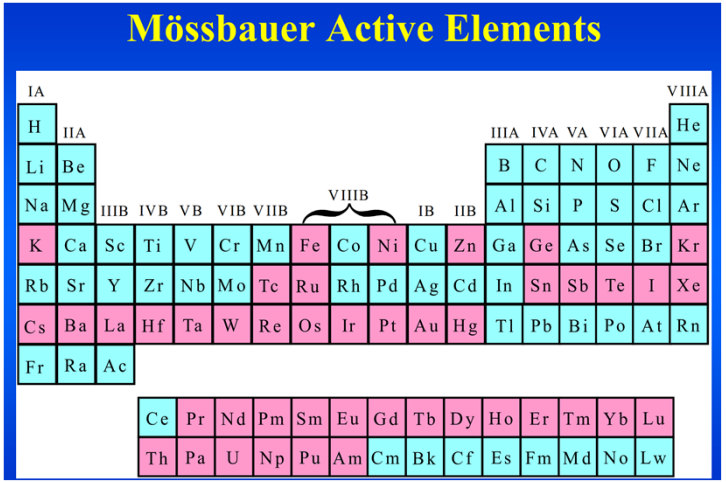

^{57}Fe, ^{119}Sn

Experimental Resonance Conditions

Transition energy: $E_\gamma = E_a - E_g$

Suitable range: $5\ keV \le E_\gamma \le 180\ keV$

If $E_\gamma \le 5$ keV: Complete non-resonance absorption

If $E_\gamma \ge 180$ keV: Recoil energy $E_R = E_\gamma^2/2mc^2$ becomes too large and destroys resonance

跃迁能高于180 KeV，会加大反冲能，从而破坏共振；小于5keV，则几乎会被全部吸收。

Nuclear parameters for selected Mössbauer isotopes

Isotope	E_γ/keV	Γ_r/(mm s^{-1}) = 2 Γ_{nat}	I_g	I_e	α	Natural abundance %	Nuclear decay*
^{57}Fe	14.41	0.192	1/2–	3/2–	8.17	2.17	^{57}Co(EC 270 d)
^{61}Ni	67.40	0.78	3/2–	5/2–	0.12	1.25	^{61}Co(β$^-$99 m)
^{119}Sn	23.87	0.626	1/2+	3/2+	5.12	8.58	^{119m}Sn(IT 50 d)
^{121}Sb	37.15	2.1	5/2+	7/2+	~10	57.25	^{121m}Sn(β$^-$76 y)
^{125}Te	35.48	5.02	1/2+	3/2+	12.7	6.99	^{125}I(EC 60d)
^{127}I	57.60	2.54	5/2+	7/2+	3.70	100	^{127m}Te (β$^-$109 d)
^{129}I	27.72	0.59	7/2+	5/2+	5.3	nil	^{129m}Te (β$^-$33 d)
^{149}Sm	22.5	1.60	7/2–	5/2–	~12	13.9	^{149}Eu(EC 106 d)
^{151}Eu	21.6	1.44	5/2+	7/2+	29	47.8	^{151}Gd(EC 120 d)
^{161}Dy	25.65	0.37	5/2+	5/2–	~2.5	18.88	^{161}Tb(β$^-$6.9 d)
^{193}Ir	73.0	0.60	3/2+	1/2+	~6	61.5	^{193}Os(β$^-$31 h)
^{197}Au	77.34	1.87	3/2+	1/2+	4.0	100	^{197}Pt(β$^-$18 h)
^{237}Np	59.54	0.067	5/2+	5/2–	1.06	nil	^{241}Am(α458 y)

*EC = electron capture, β$^-$ = beta-decay, IT = isomeric transition, α – alpha-decay

(1) 同质异能位移

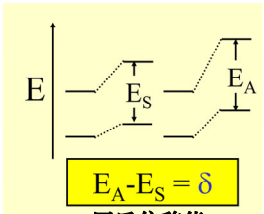

同质位移能

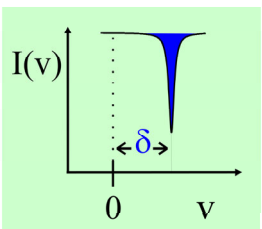

核电荷分布程球对称

(2) 四极分裂

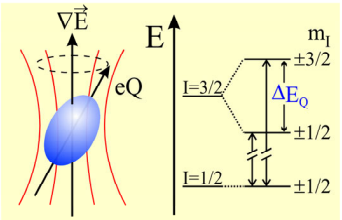

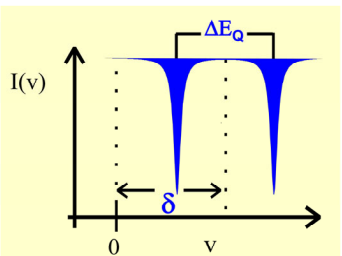

核电荷分布偏离球对称

(2) 磁超精细分裂

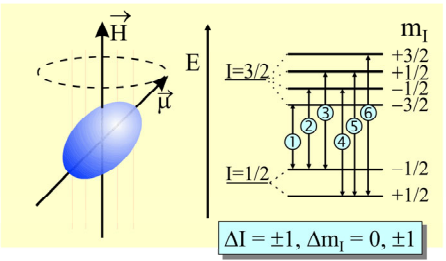

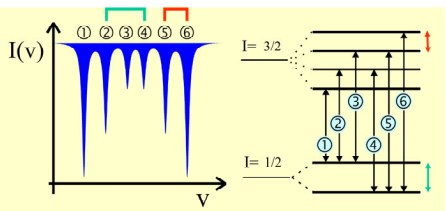

原子核处于磁场

JACS
JOURNAL OF THE AMERICAN CHEMICAL SOCIETY
Article
pubs.acs.org/JACS

A Combined Mössbauer, Magnetic Circular Dichroism, and Density Functional Theory Approach for Iron Cross-Coupling Catalysis: Electronic Structure, In Situ Formation, and Reactivity of Iron-Mesityl-Bisphosphines

Stephanie L. Daifuku,† Malik H. Al-Afyouni,† Benjamin E. R. Snyder, Jared L. Kneebone, and Michael L. Neidig*

Department of Chemistry, University of Rochester, Rochester, New York 14627, United States

Supporting Information

ABSTRACT: While iron-bisphosphines have emerged as effective catalysts for C−C cross-coupling, the nature of the in situ formed iron species, elucidation of the active catalysts and the mechanisms of catalysis have remained elusive. A combination of ^{57}Fe Mössbauer and magnetic circular dichroism (MCD) spectroscopies of well-defined and in situ formed mesityl-iron(II)-SciOPP species combined with density functional theory (DFT) investigations provides the first direct insight into electronic structure, bonding and in situ speciation of mesityl-iron(II)-bisphosphines in the Kumada cross-coupling of MesMgBr and primary alkyl halides using $FeCl_2$(SciOPP). Combined with freeze-trapped solution Mössbauer studies of reactions with primary alkyl halides, these studies demonstrate that distorted square-planar $FeMes_2$(SciOPP) is the active catalyst for cross-coupling and provide insight into the molecular-level mechanism of catalysis. These studies also define the effects of key reaction protocol details, including the role of the slow Grignard addition method and the addition of excess SciOPP ligand, in leading to high product yields and selectivities.

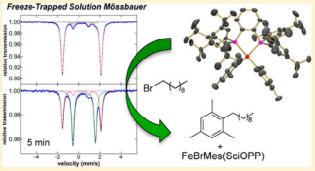

Scheme 1. $FeCl_2$(SciOPP) Catalyzed C–C Cross-Couplings

(a) Kumada (Nakamura 2011)

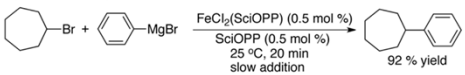

(b) Suzuki-Miyaura (Nakamura 2010)

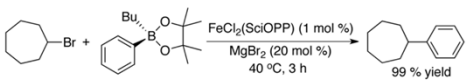

(c) Sonogashira-type (Nakamura 2011)

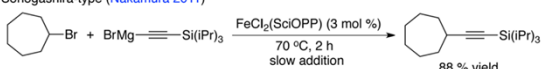

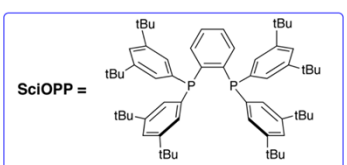

Scheme 2. $FeCl_2$(SciOPP) Catalyzed Kumada Cross-Coupling of MesMgBr and Primary Alkyl Halides[18]

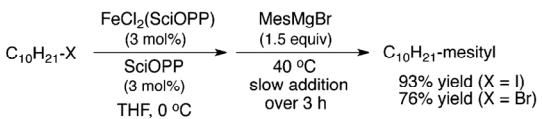

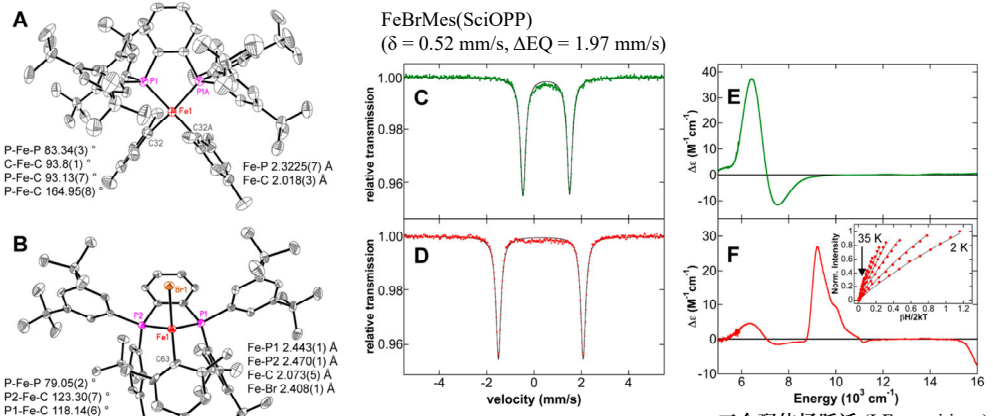

畸变的四面体

Figure 1. X-ray, Mössbauer, and MCD characterization of mesityl-iron(II)-SciOPP complexes X-ray crystal structures of (A) $FeMes_2$(SciOPP) and (B) FeMesBr(SciOPP). Select bond distances and angles are given for each structure, and thermal ellipsoids are shown at the 50% probability level. 80 K Mössbauer spectrum of solid (C) FeBrMes(SciOPP) and (D) $FeMes_2$(SciOPP). 5 K, 7 T NIR MCD spectrum of (E) FeBrMes(SciOPP) and (F) $FeMes_2$(SciOPP). (F, inset) VTVH-MCD data (dots) and fit (lines) of $FeMes_2$(SciOPP) collected at 10 000 cm^{-1}. 近红外-磁性圆二色谱可变场-磁性圆二色谱

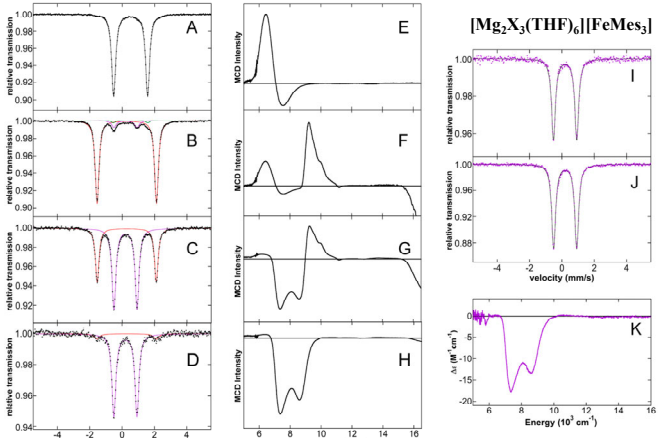

Figure 4. ^{57}Fe Mössbauer and NIR MCD spectroscopy of in situ formed iron species in reactions of $^{57}FeCl_2$(SciOPP) with MesMgBr. (A–D) 80 K ^{57}Fe Mössbauer spectra from reaction of $FeCl_2$(SciOPP) (3 mM) with (A) 1 equiv, (B) 2 equiv, (C) 20 equiv and (D) 100 equiv of MesMgBr. Data (black dots) and total fit (black lines) are shown. Individual component fits are shown and described in the text. (E–H) 5 K, 7 T NIR MCD spectra from reaction of $FeCl_2$(SciOPP) (3 mM) with (E) 1 equiv, (F) 2 equiv, (G) 20 equiv and (H) 100 equiv of MesMgBr. (I) 80 K ^{57}Fe Mössbauer spectrum of solid $FeMes_3^-$. (J) 80 K ^{57}Fe Mössbauer spectrum of in situ generated $FeMes_3^-$ from reaction of $^{57}FeCl_2$·1.5THF (3 mM) with 3 equiv of MesMgBr. (G) 5 K, 7 T NIR MCD spectrum of $FeMes_3^-$ (3 mM). All solution samples were prepared in 1:1 THF:2-MeTHF. Mössbauer fit analysis errors are $\delta \pm 0.02$ mm/s, $\Delta E_Q \pm 2\%$ and percentage of total iron $\pm 3\%$.

Table 1. ^{57}Fe Mössbauer Parameters for Iron-SciOPP and Iron-Mesityl Complexes

complex	sample	isomer shift (δ)[c]	ΔE_Q[c]
$FeCl_2$(SciOPP)[a]	frozen solution[b]	0.94 mm/s	2.69 mm/s
$FeBr_2$(SciOPP)[a]	frozen solution	0.92 mm/s	2.95 mm/s
FeBrMes(SciOPP)	solid	0.52 mm/s	1.97 mm/s
FeBrMes(SciOPP)	frozen solution	0.52 mm/s	2.12 mm/s
FeClMes(SciOPP)[a]	solid	0.53 mm/s	1.87 mm/s
$FeMes_2$(SciOPP)	solid	0.29 mm/s	3.58 mm/s
$FeMes_2$(SciOPP)	frozen solution	0.28 mm/s	3.67 mm/s
$FeMes_3^-$	solid	0.20 mm/s	1.44 mm/s
$FeMes_3^-$	frozen solution	0.21 mm/s	1.43 mm/s

[a]Mössbauer spectra are given in the SI. [b]All frozen solution samples prepared with ^{57}Fe enriched complex at 3 mM in 1:1 THF:2-MeTHF. [c]Mössbauer fitting errors are ± 0.02 mm/s for δ and $\pm 2\%$ for ΔE_Q.

Scheme 3. In Situ Iron Speciation from Reaction of $FeCl_2$(SciOPP) with MesMgBr

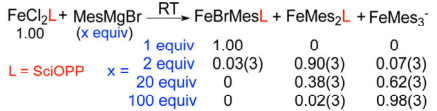

$FeMes_2$(SciOPP)

FeXMes(SciOPP)

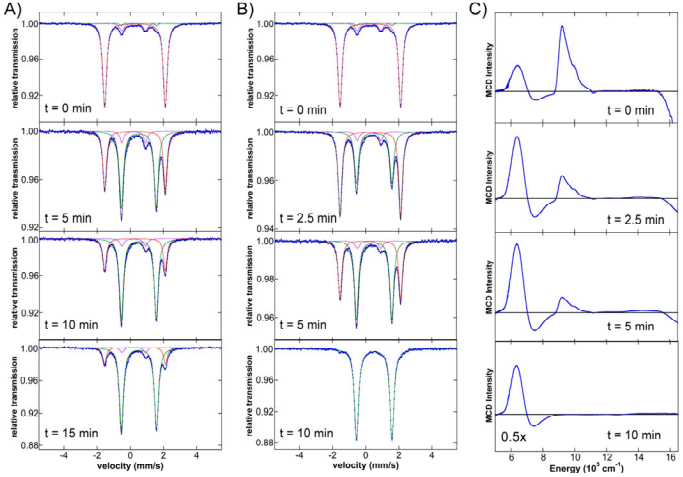

分别加入1-溴癸烷和1-碘癸烷原位监控反应

Figure 7. ^{57}Fe Mössbauer and MCD spectroscopy of the iron species present in situ in reactions of solution generated $FeMes_2$(SciOPP) with primary alkyl halides. 80 K ^{57}Fe Mössbauer spectrum of in situ generated $FeMes_2$(SciOPP)$_2$ in 1:1 THF:2-MeTHF and the spectra of freeze-trapped samples as a function of time following reaction with (A) 20 equiv of 1-bromodecane and (B) 20 equiv of 1-iododecane. Data (black dots) and total fits (black lines) are shown for each spectrum. Details of the individual components are given in the SI. (C) The 5 K, 7 T NIR MCD spectrum of in situ generated $FeMes_2$(SciOPP)$_2$ in 1:1 THF:2-MeTHF and the spectra of freeze-trapped samples as a function of time following reaction with 1-iododecane. All MCD spectra are shown with the same *y*-axis scale for direct comparison (the 10 min spectrum is shown at half-intensity to fit on the same scale).

Scheme 5. Proposed Mechanism by Nakamura for $FeCl_2$(SciOPP) Catalyzed Cross-Coupling of Aryl Nucleophiles and Alkyl Electrophiles[17,18]

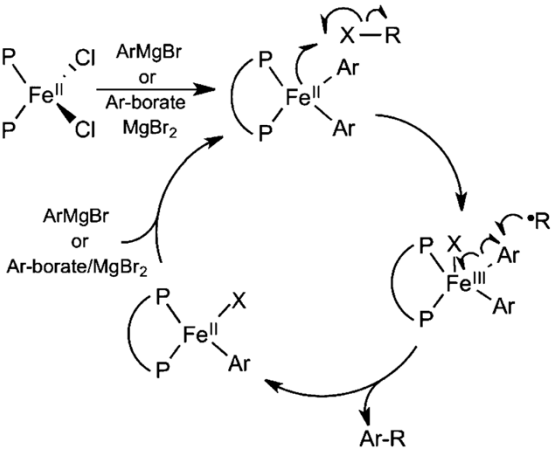

JACS
JOURNAL OF THE AMERICAN CHEMICAL SOCIETY
Article
pubs.acs.org/JACS

Iron(II) Active Species in Iron–Bisphosphine Catalyzed Kumada and Suzuki–Miyaura Cross-Couplings of Phenyl Nucleophiles and Secondary Alkyl Halides

Stephanie L. Daifuku, Jared L. Kneebone, Benjamin E. R. Snyder, and Michael L. Neidig*

Department of Chemistry, University of Rochester, Rochester, New York 14627, United States

Supporting Information

ABSTRACT: While previous studies have identified Fe-Mes_2(SciOPP) as the active catalyst species in iron–SciOPP catalyzed Kumada cross-coupling of mesitylmagnesium bromide and primary alkyl halides, the active catalyst species in cross-couplings with phenyl nucleophiles, where low valent iron species might be prevalent due to accessible reductive elimination pathways, remains undefined. In the present study, in situ Mössbauer and magnetic circular dichroism spectroscopic studies combined with inorganic syntheses and reaction studies are employed to evaluate the in situ formed iron species and identify the active catalytic species in iron–SciOPP catalyzed Suzuki–Miyaura and Kumada cross-couplings of phenyl nucleophiles and secondary alkyl halides. While reductive elimination to form Fe(η^6-biphenyl)(SciOPP) occurs upon reaction of $FeCl_2$(SciOPP) with phenyl nucleophiles, this iron(0) species is not found to be kinetically competent for catalysis. Importantly, mono- and bis-phenylated iron(II)–SciOPP species that form prior to reductive elimination are identified, where both species are found to be reactive toward electrophile at catalytically relevant rates. The higher selectivity toward the formation of cross-coupled product observed for the monophenylated species combined with the undertransmetalated nature of the in situ iron species in both Kumada and Suzuki–Miyaura reactions indicates that Fe(Ph)X(SciOPP) (X = Br, Cl) is the predominant reactive species in cross-coupling. Overall, these studies demonstrate that low-valent iron is not required for the generation of highly reactive species for effective aryl-alkyl cross-couplings.

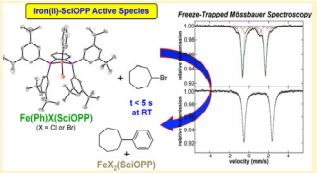

J. Am. Chem. Soc. **2015**, *137*, 11432.

Scheme 1. Representative Iron−Bisphosphine Catalyzed Cross-Coupling Reactions

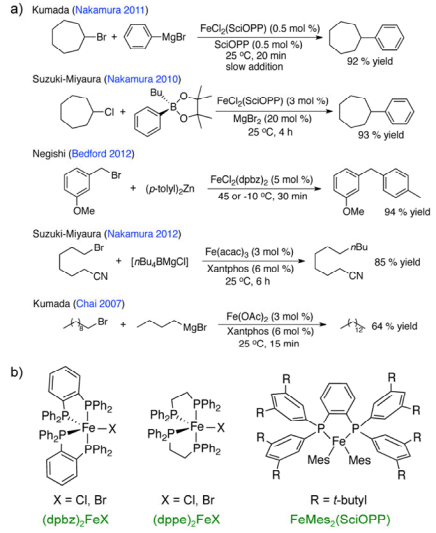

Scheme 2. Proposed Mechanism by Nakamura and Co-workers for $FeCl_2$(SciOPP) Catalyzed Cross-Coupling of Aryl Nucleophiles and Alkyl Electrophiles[42,43]

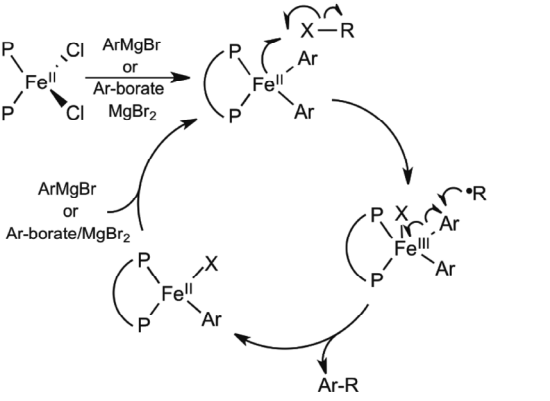

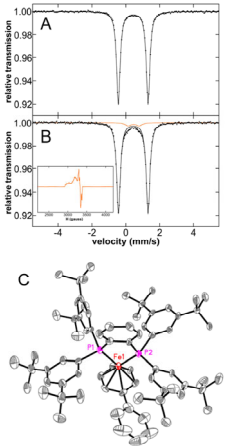

Figure 1. Formation of low-valent iron species upon reaction of $FeCl_2$(SciOPP) (**1**-Cl_2) with phenyl nucleophiles. The 80 K Mössbauer spectra of the in situ iron species from reaction of ^{57}Fe–**1**-Cl_2 with (A) 20 equiv *t*BuPh-borate/6.7 equiv $MgBr_2$ and (B) 2 equiv PhMgBr at 25 °C. The minor $S = 1/2$ component (**3**) observed by 10 K EPR spectroscopy upon reaction with PhMgBr (~5% of all iron present) is shown in the inset of (B). (C) X-ray crystal structure of Fe(η^6-biphenyl)(SciOPP) (**2**) with thermal ellipsoids shown at 50% probability.

Table 1. Suzuki–Miyaura Cross-Couplings with $FeCl_2$(SciOPP) (1**-Cl_2) and Fe(η^6-Biphenyl)(SciOPP) (**2**) Precatalysts**

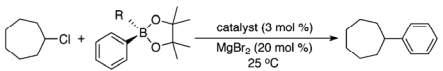

catalyst	R	time (h)	Chp-Ph yield (%)	ChpCl (unreacted) (%)
1-Cl_2	*n*-butyl	4	93[a]	0
	t-butyl	4	89	2
2	*t*-butyl	4	63	32
	t-butyl	6	83	17

[a]The results with R = *n*-butyl are from ref 42.

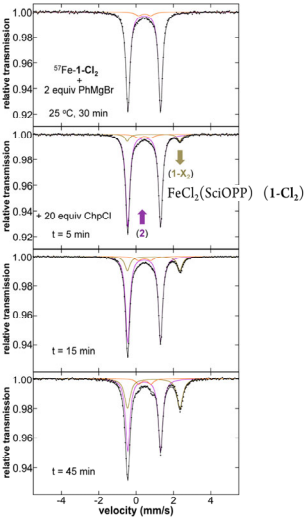

Figure 2. The 80 K Mössbauer spectra of the in situ iron species as a function of reaction time during the reaction of Fe(η^6-biphenyl)(SciOPP) (**2**) with chlorocycloheptane. The individual ^{57}Fe Mössbauer components are identified as **2** (purple), **1**-X_2 (beige), and **3** (orange).

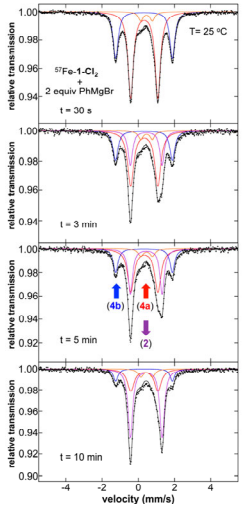

Figure 4. The 80 K Mössbauer spectra of the in situ iron species as a function of reaction time at 25 °C from reaction of $^{57}FeCl_2$(SciOPP) (^{57}Fe−**1**-Cl$_2$) with 2 equiv PhMgBr in 1:1 THF/2-MeTHF. The individual Mössbauer components are identified as **4a** (red), **4b** (blue), **3** (orange), and **2** (purple).

Table 2. Mössbauer Parameters of Mesitylated Iron(II)−Bisphosphine Complexes[50,51]

complex	geometry	sample	δ (mm/s)	ΔE_Q (mm/s)
$FeMes_2$(SciOPP)	sq. planar	solid	0.29	3.58
		froz. soln.	0.28	3.67
$FeMes_2(PEt_2Ph)_2$	sq. planar	solid	0.31	4.63
$FeMes_2$(dppe)	sq. planar	solid	0.33	4.53
$FeMes_2$(depe)	dist. tetra.	solid	0.39	1.71
FeMesBr(SciOPP)	dist. tetra	solid	0.52	1.97
		froz. soln.	0.52	2.12

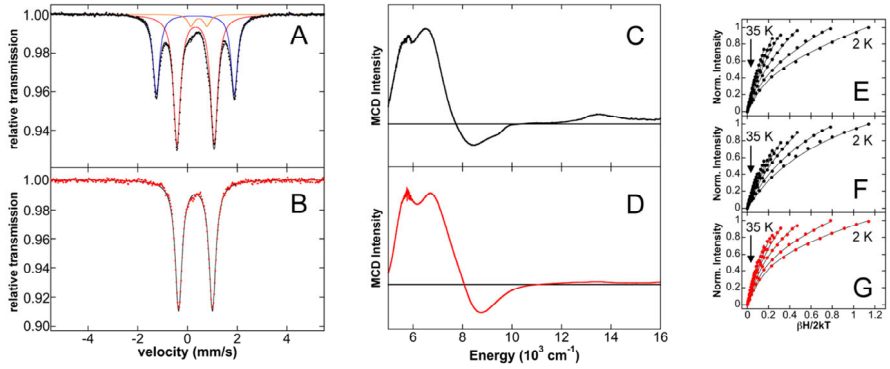

Figure 5. Mössbauer and MCD characterization of the in situ formed iron species from the reaction of $^{57}FeCl_2$(SciOPP) (^{57}Fe**−1-Cl$_2$**) with 2 equiv PhMgBr at 0 °C. (A and B) The 80 K Mössbauer and (C and D) 5 K, 7T NIR MCD spectra of the in situ iron species from reaction in (A and C) 1:1 THF/2-MeTHF and (B and D) 1:1 Et_2O/isopentane. Saturation magnetization data (dots) and best fit (lines) collected at (E) 5260 cm^{-1} and (F) 13333 cm^{-1} in 1:1 THF/2-MeTHF and at (G) 5320 cm^{-1} in 1:1 Et_2O/isopentane. The individual Mössbauer components in (A) are identified as **4a** (red), **4b** (blue), and **3** (orange).

Fe-$(Ph)_2$(SciOPP) (4a); Fe$(Ph)_2$(THF)(SciOPP) (4b)

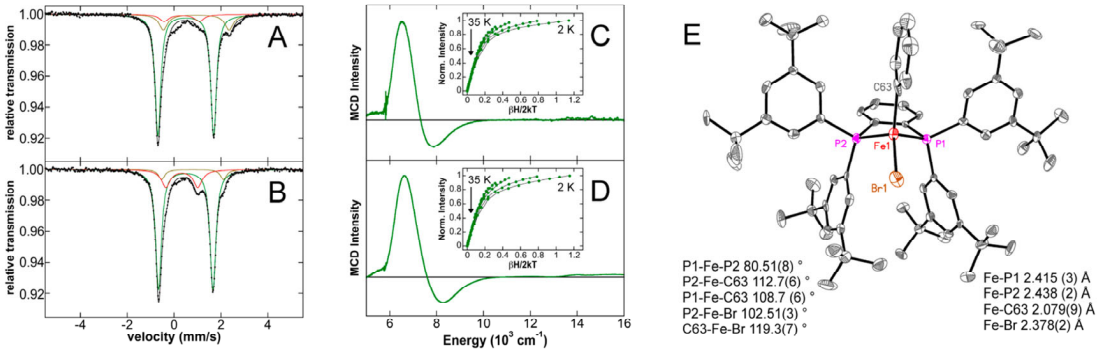

Figure 6. Spectroscopic and structural characterization of Fe(Ph)Br(SciOPP) (**5-Br**). (A and B) The 80 K Mössbauer and (C and D) 5 K, 7T NIR MCD spectra of the in situ iron species from reaction of **1-Br$_2$** with 1 equiv PhMgBr for 3 min at 0 °C in (A and C) 1:1 THF/2-MeTHF and (B and D) 1:1 Et$_2$O/isopentane. Saturation magnetization data (dots) and best fit (lines) collected at 6100 cm^{-1} (C, inset) and 6120 cm^{-1} (D, inset). (E) X-ray crystal structure of **5-Br** with thermal ellipsoids shown at 50% probability. The individual Mössbauer components are identified as **5-Br** (green), **4a** (red), and **1-Br$_2$** (beige).

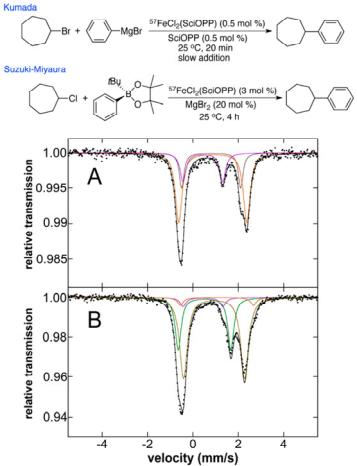

Figure 8. The 80 K Mössbauer spectra of the iron species in solution during catalysis upon freeze-trapping during (A) the Kumada reaction at t = 5 min and (B) the Suzuki–Miyaura reaction at t = 45 min of reaction time. The individual Mössbauer components are identified as **2** (purple), **5-X** (green), and **1-X$_2$** species (beige/orange).

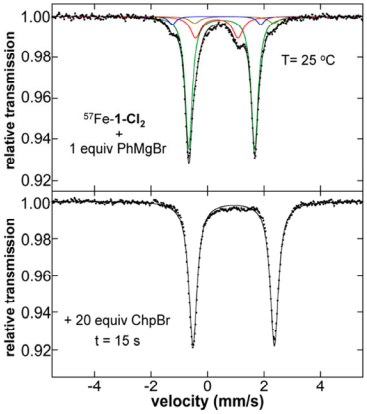

Figure 9. The 80 K Mössbauer spectra of the iron species in solution (A) following reaction of $^{57}FeCl_2$(SciOPP) (^{57}Fe−**1-Cl$_2$**) with 1 equiv PhMgBr at 25 °C in 1:1 THF/2-MeTHF for 1 min and (B) after subsequent addition of 20 equiv bromocycloheptane and reaction for 15 s. The individual Mössbauer components are identified as **4a** (red), **4b** (blue), **5-X** (green), and **1-X$_2$** (beige).

Scheme 3. Major Iron Species Formed in Situ and Their Reaction Pathways for the $FeCl_2$(SciOPP) (1-Cl_2) Catalyzed Kumada and Suzuki–Miyaura Cross-Couplings of Phenyl Nucleophiles and Secondary Alkyl Halides[a]

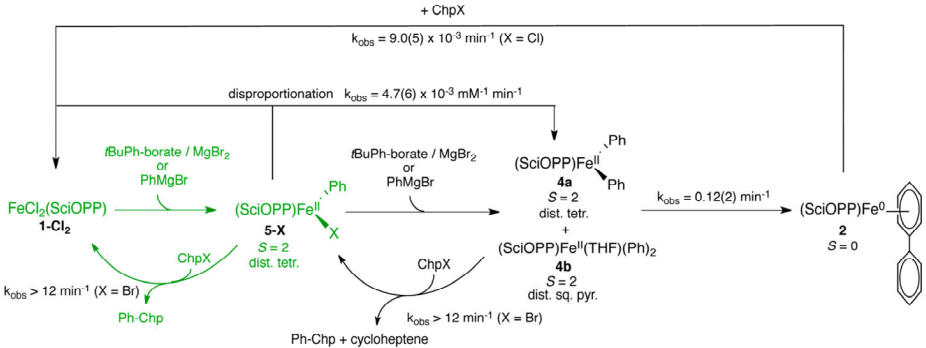

[a]Estimated rates are given for the transformations at 25 °C.

JACS
JOURNAL OF THE AMERICAN CHEMICAL SOCIETY
Article
pubs.acs.org/JACS

Intermediates and Reactivity in Iron-Catalyzed Cross-Couplings of Alkynyl Grignards with Alkyl Halides

Jared L. Kneebone, William W. Brennessel, and Michael L. Neidig*

Department of Chemistry, University of Rochester, Rochester, New York 14627, United States

Supporting Information

ABSTRACT: Iron-catalyzed cross-coupling reactions using alkynyl nucleophiles represent an attractive approach for the incorporation of alkynyl moieties into organic molecules. In the present study, a multitechnique approach combining inorganic spectroscopic methods, inorganic synthesis, and reaction studies is applied to iron-SciOPP catalyzed alkynyl-alkyl cross-couplings, providing the first detailed insight into the effects of variation from *sp*³- to *sp*-hybridized nucleophiles on iron speciation and reactivity. Reaction studies demonstrate that reaction of $FeBr_2$(SciOPP) with 1 equiv (triisopropylsilyl)ethynylmagnesium bromide (TIPS-CC-MgBr) leads to a distribution of mono-, bis-, and tris-alkynylated iron(II)-SciOPP species due to rapid alkynyl ligand redistribution.

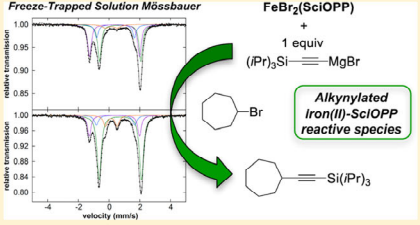

J. Am. Chem. Soc. **2017**, *139*, 6988.

Scheme 1. Examples of Iron-Catalyzed $C(sp)-C(sp^3)$ Cross-Coupling Reactions

Nakamura and co-workers (refs. 44, 45)

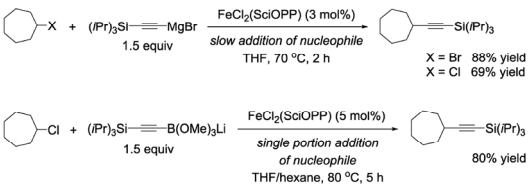

Hu and co-workers (ref. 46)

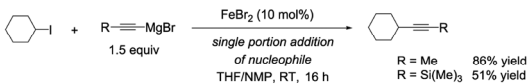

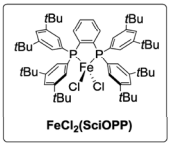

Scheme 2. Catalytic Cycle Proposed by Nakamura and Co-workers for the Cross-Coupling of Alkynyl Grignards with Alkyl Halides Catalyzed by $FeCl_2$(SciOPP)

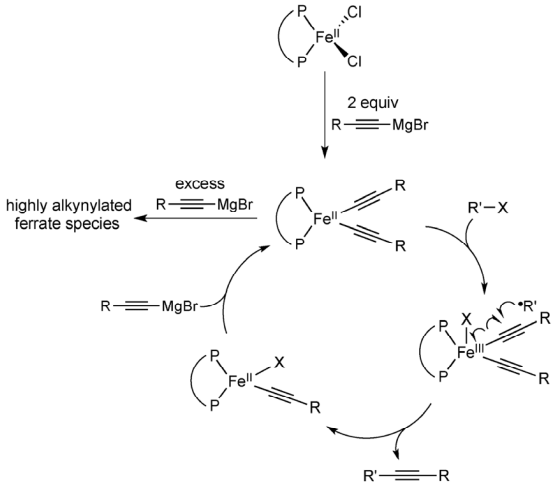

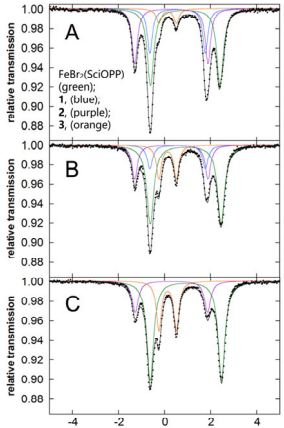

1: [Fe(CC-TIPS)X)(SciOPP)]-[MgBr] **2**: [Fe(CC-TIPS)$_2$)(SciOPP)]-[MgBr]

Figure 1. 5 K frozen solution Mössbauer spectra of the in situ generated iron distribution formed upon reaction of $^{57}FeBr_2$(SciOPP) with 1 equiv of TIPS-CC-MgBr in 1:1 THF/2-MeTHF at room temperature after (A) 1 min, (B) 5 min, and (C) 30 min of reaction time. Assignments of individual doublets and their relative percentages in each spectrum are as follows: (A) $^{57}FeBr_2$(SciOPP)$_2$, 45% (green); **1**, 21% (blue); **2**, 26% (purple); **3**, 8% (orange). (B) $^{57}FeBr_2$(SciOPP), 53% (green); **1**, 13% (blue); **2**, 18% (purple); **3**, 16% (orange). (C) $^{57}FeBr_2$(SciOPP), 61% (green); **2**, 17% (purple); **3**, 22% (orange).

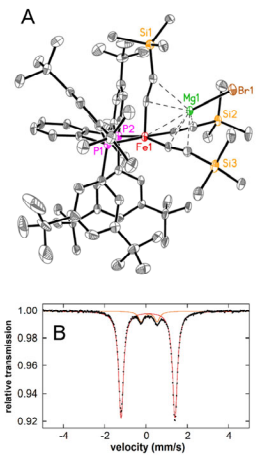

Figure 2. Solid state characterization of **3**. (A) X-ray crystal structure of **3** with thermal ellipsoids drawn at the 50% probability level. Hydrogen atoms as well as the terminal methyl groups of the (triisopropylsilyl)ethynyl ligands have been removed for clarity. (B) 5 K Mössbauer spectrum of solid **3** isolated from the reaction of $^{57}FeBr_2$(SciOPP) with 3 equiv of TIPS-CC-MgBr (Grignard reagent prepared in Et_2O) at room temperature in 1:1 (v:v) Et_2O/isopentane. Assignments of the doublets and their relative percentages in Figure 2B are as follows: δ = 0.10 mm/s, ΔE_Q = 2.61 mm/s (red, 90%), and δ = 0.14 mm/s and ΔE_Q = 0.76 mm/s (orange, 10%).

A [Fe(CC-TIPS)$_3$(η^1-N$_2$)(SciOPP)][MgBr] (**3-N2**)

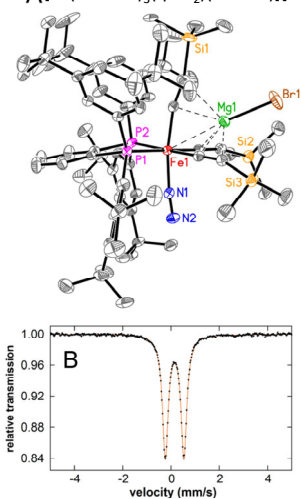

Figure 3. Solid state characterization of **3-N$_2$**. (A) X-ray crystal structure of **3-N$_2$** with thermal ellipsoids drawn at the 50% probability level. Hydrogen atoms as well as the terminal methyl groups of the (triisopropylsilyl)ethynyl ligands have been removed for clarity. (B) 5

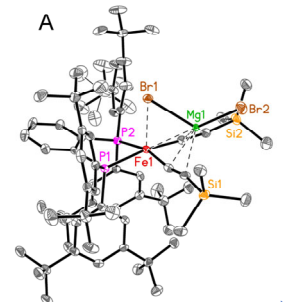

Figure 5. Solid state characterization of **2**. (A) X-ray crystal structure of **2** with thermal ellipsoids drawn at the 50% probability level. Hydrogen atoms as well as the terminal methyl groups of the (triisopropylsilyl)ethynyl ligands have been removed for clarity. (B) 5 K Mössbauer spectrum of solid **2**, characterized by a doublet with δ = 0.36 mm/s and ΔE_Q = 3.32 mm/s.

Table 1. Summary of Mössbauer Parameters of Alkynylated and Phenylated Iron(II)-SciOPP Species[a]

complex	sample[b]	δ (mm/s)	ΔE_Q (mm/s)
Alkynylated iron(II)-SciOPP *(this work)*			
Fe(CC-TIPS)Br(SciOPP) (**1**)	frozen soln	0.57	2.41
$Fe(CC\text{-}TIPS)_2(SciOPP)$ (**2**)	frozen soln	0.31	3.18
	solid	0.36	3.32
$[Fe(CC\text{-}TIPS)_3(SciOPP)][MgBr]$ (**3**)	solid	0.10	2.61
$[Fe(CC\text{-}TIPS)_3(\eta^1\text{-}N_2)(SciOPP)][MgBr]$ (**3-N_2**)	frozen soln	0.14	0.76
	solid	0.14	0.76
Phenylated iron(II)-SciOPP *(ref 49)*			
Fe(Ph)Br(SciOPP)	frozen soln	0.50	2.37
$Fe(Ph)_2(THF)(SciOPP)$	frozen soln	0.32	3.13
$Fe(Ph)_2(SciOPP)$	frozen soln	0.33	1.50

[a]All spectra were collected at 5 K. [b]All frozen solution spectra were acquired on 1:1 THF/2-MeTHF frozen solution samples.

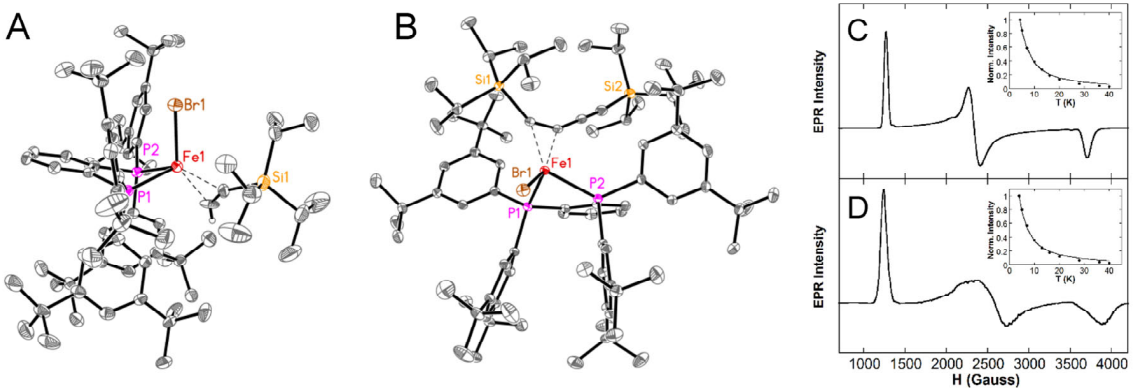

Figure 8. Solid state and spectroscopic characterization of **4** and **5**. X-ray crystal structures of (A) **4** and (B) **5** with thermal ellipsoids drawn at the 50% probability level and hydrogen atoms omitted for clarity. 5 K EPR spectra of (C) **4** and (D) **5** in 1:1 THF/2-MeTHF and the temperature dependence of the $S = 3/2$ signal intensity for **4** (C, inset) and **5** (D, inset).

4和5无反应活性

1和2为反应活性物种，3无反应活性

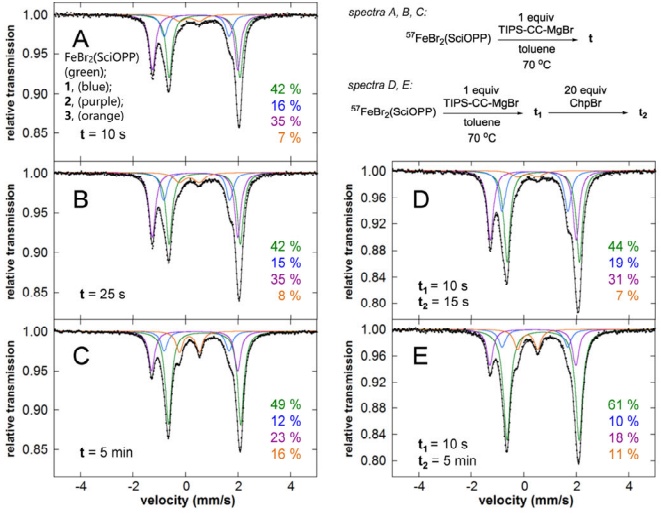

Figure 9. 5 K frozen solution Mössbauer spectra showing the in situ generated iron distribution resulting from reaction of $^{57}FeBr_2$(SciOPP) with 1 equiv of Et_2O-based TIPS-CC-MgBr in toluene at 70 °C over (A) 10 s, (B) 25 s, and (C) 5 min. Reaction of the distribution in spectrum A with 20 equiv cycloheptyl bromide for (D) 15 s and (E) 5 min demonstrates consumption of **1** (blue doublet) and **2** (purple doublet) following addition of cycloheptyl bromide. Table S1 displays the individual parameters and relative percentages for all species in each spectrum in tabular form.

GDCh Research Article Angewandte International Edition Chemie www.angewandte.org

How to cite: *Angew. Chem. Int. Ed.* **2025**, *64*, e202413566
doi.org/10.1002/anie.202413566

Cross-coupling reactions

Effective Alkyl-Alkyl Cross-Coupling with an Iron-Xantphos Catalyst: Mechanistic and Structural Insights

*Magali Gimeno[+], Maria Camila Aguilera[+], Valerie E. Fleischauer, William W. Brennessel, and Michael L. Neidig**

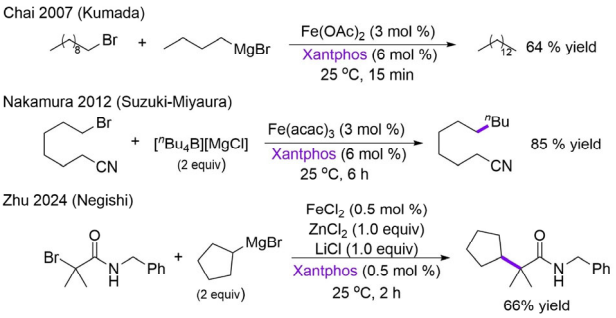

Scheme 1. Representative examples of iron-catalyzed alkyl-alkyl cross-coupling reactions using Xantphos as supporting ligand.

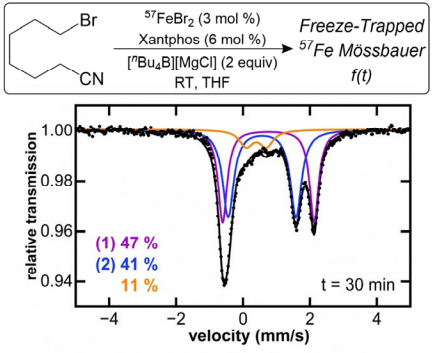

Figure 1. Freeze-trapped 80 K ^{57}Fe Mössbauer spectra of iron speciation during catalysis in THF. Mössbauer parameters for purple component (**1**) $\delta = 0.78$ mm/s $|\Delta E_Q| = 2.76$ mm/s, blue component (**2**) $\delta = 0.55$ mm/s $|\Delta E_Q| = 2.05$ mm/s and orange component $\delta = 0.41$ mm/s $|\Delta E_Q| = 0.64$ mm/s.

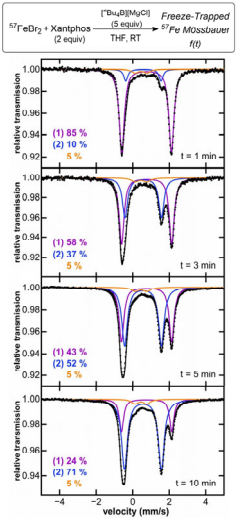

Figure 2. Freeze-trapped 80 K ^{57}Fe Mössbauer spectra of reaction of Fe(Xantphos)Br$_2$ with ^{t}butylborane. Mössbauer parameters for purple component $\delta = 0.78$ mm/s $|\Delta E_Q| = 2.76$ mm/s (**1-Br**), blue component $\delta = 0.55$ mm/s $|\Delta E_Q| = 2.05$ mm/s (**2**), orange component $\delta = 0.41$ mm/s $|\Delta E_Q| = 0.64$ mm/s.

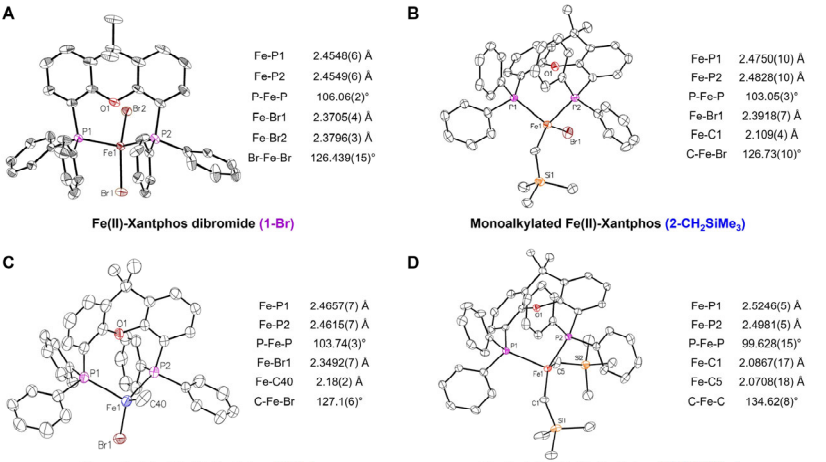

Figure 3. SC-XRD of isolated crystalline material of iron(II) Xantphos intermediates. A) Fe(II) Xantphos dibromide (**1-Br**). B) Monoalkylated Fe(II)–Xantphos (**2-CH$_2$SiMe$_3$**). C) Monoalkylated Fe(II)–Xantphos (**2-Me**). D) Bisalkylated Fe(II)–Xantphos (**3-CH$_2$SiMe$_3$**). Thermal ellipsoids are shown at 50% probability.[58]

1: (Fe(Xantphos)Br$_2$; 2: (Fe(Xantphos)(Et)Br; 2的单晶无法得到。

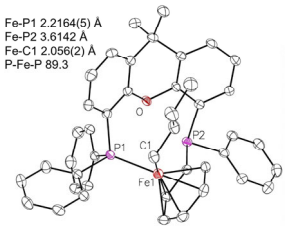

(4) Fe(^{n}Bu)(κ^2P:(η^6-C_6H_5)-Xantphos

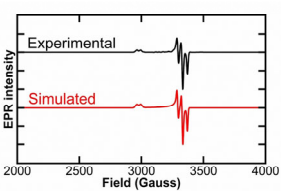

Figure 5. EPR characterization of **4**, Fe(I) $S = 1/2$. Simulated g values of $g_1 = 2.25$, $g_2 = 2.02$and $g_3 = 1.99$, and hyperfine coupling to the ^{31}P from the Xantphos ligand with constant $A_1 = 111.4$, $A_2 = 91.9$ and $A_3 = 102.5$ MHz. Thermal ellipsoids of **4** are shown at 50% of probability.[58] Fe–C (phenyl ring) bond length range 2.0853(19) – 2.136(2) Å.

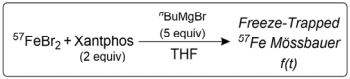

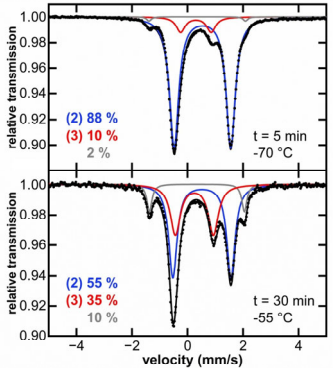

Figure 4. Freeze-trapped 80 K ^{57}Fe Mössbauer spectra of reaction of **1** with 5 equiv. of ^{n}BuMgBr. The reaction time and temperature are indicated within each spectrum. Parameters for blue component $\delta = 0.55$ mm/s $|\Delta E_Q| = 2.05$ mm/s (**2**), red component $\delta = 0.25$ mm/s $|\Delta E_Q| = 1.33$ mm/s (**3**), grey component $\delta = 0.34$ mm/s $|\Delta E_Q| = 3.47$ mm/s.

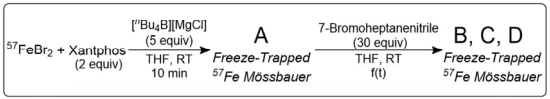

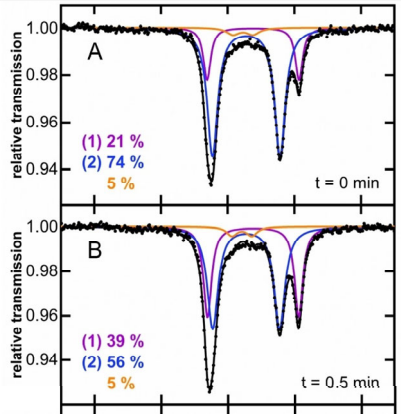

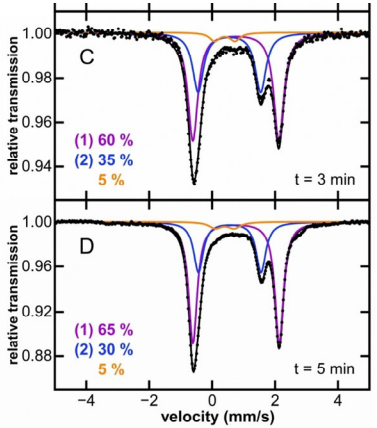

Figure 6. Freeze-trapped 80 K ^{57}Fe Mössbauer spectra of the in situ formed iron species upon reaction of $^{57}FeBr_2$ and 2 equiv. of Xantphos, with 5 equiv. of [^{n}Bu$_4$B][MgCl] for 10 min (A) and following subsequent reaction with 7-bromoheptanenitrile at different timepoints (B, C & D).

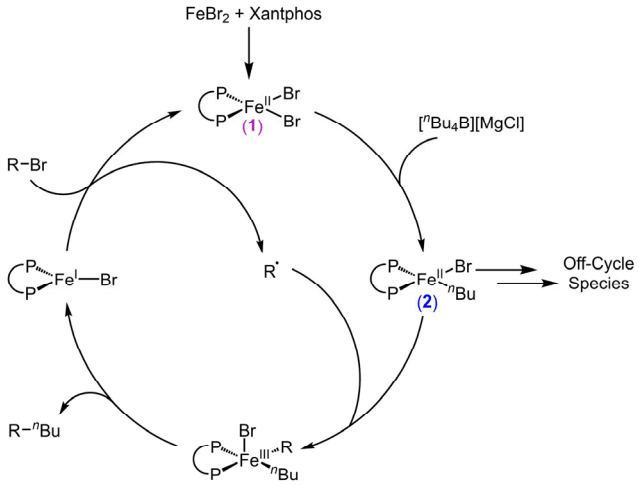

Scheme 2. Proposed mechanistic cycle for Fe-Xantphos catalyzed C-(sp^3)–C(sp^3) cross-couplings.

JACS
JOURNAL OF THE AMERICAN CHEMICAL SOCIETY
Communication
pubs.acs.org/JACS

Isolation and Characterization of a Tetramethyliron(III) Ferrate: An Intermediate in the Reduction Pathway of Ferric Salts with MeMgBr

Malik H. Al-Afyouni, Kathlyn L. Fillman, William W. Brennessel, and Michael L. Neidig*

Department of Chemistry, University of Rochester, Rochester, New York 14627, United States

Supporting Information

ABSTRACT: While iron-catalyzed Kumada cross-coupling reactions with simple iron salts have been known since the early 1970s, the nature of the *in situ*-formed iron species remains elusive. Herein, we report the synthesis of the homoleptic tetralkyliron(III) ferrate complex $[MgCl(THF)_5][FeMe_4]$ from the reaction of $FeCl_3$ with MeMgBr in THF. Upon warming, this distorted square-planar $S = {}^3/_2$ species converts to the $S = {}^1/_2$ species originally observed by Kochi and co-workers with concomitant formation of ethane, consistent with its intermediacy in the reduction pathway of $FeCl_3$ to generate the reduced iron species involved in catalysis.

Scheme 1

Kochi (1971)

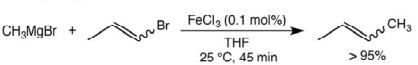

Fürstner (2006)

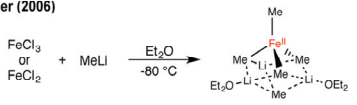

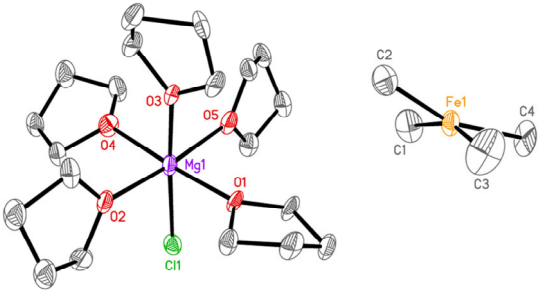

Figure 1. Crystal structure of **1**. Thermal ellipsoids are shown at 50% probability. H atoms and non-coordinated solvent are omitted for clarity. Selected bond lengths and angles: Fe1−C1 = 2.04(1) Å, Fe1−C2 = 2.05(1) Å, Fe1−C3 = 2.01(1) Å, Fe1−C4 = 2.05(1) Å, C1−Fe1−C2 = 94.7(7)°, C2−Fe1−C3 = 89.7(7)°, C3−Fe1−C4 = 91.1(7)°, C1−Fe1−C4 = 91.4(6)°, C1−Fe1−C3 = 158.7(7)°, C2−Fe1−C4 = 161.0(6)°. Note that the halide in the cation occurs in a ~0.4:0.6 ratio of Br:Cl in the crystal structure.

The addition of 4 equiv of methylmagnesium bromide to ferric chloride in THF at −80 °C results in a color change from green to orange. Despite the numerous difficulties in handling this highly air-, moisture-, and temperature-sensitive product, single orange crystals of **1** suitable for X-ray crystallography grown from a THF/hexane mixture at −80 °C reveal the iron-containing species to be $[MgCl(THF)_5][FeMe_4]\cdot THF$ (Figure 1). The

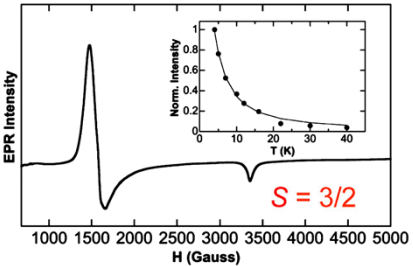

Figure 2. 10 K EPR spectrum of **1** in THF generated from reaction of $FeCl_3$ with MeMgBr. Inset shows the temperature-dependent EPR intensity of **1** and Boltzmann fit to the Curie law to give an axial ZFS parameter of $D = 6.5 \pm 0.5$ cm^{-1}.

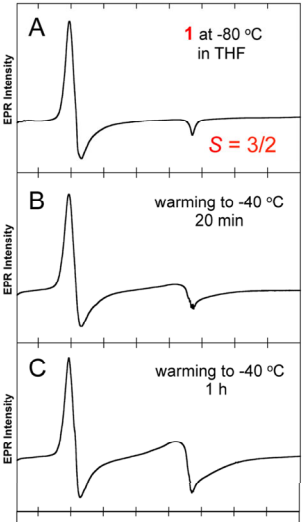

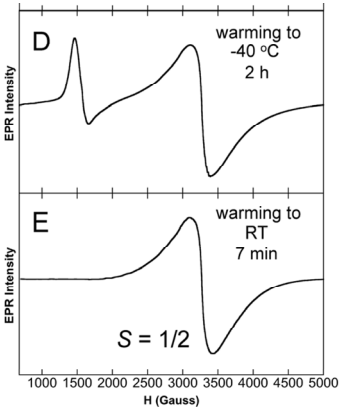

Figure 4. 10 K EPR spectra of the iron species in solution upon warming **1** in THF. (A) **1** in THF at −80 °C. (B–D) Warming **1** from −80 to −40 °C for (B) 20 min, (C) 1 h, and (D) 2 h. (E) Warming **1** from −80 °C to room temperature for 7 min. All samples were freeze-trapped in liquid nitrogen at the designated time points.

Scheme 2

Kochi et al.

$$FeCl_3 + CH_3MgBr \xrightarrow[\text{-40 °C to RT}]{\text{THF}} S = 1/2\ (\text{EPR}) \quad (-CH_3CH_3)$$

This work

$$FeCl_3 + CH_3MgBr \xrightarrow[\text{-80 °C}]{\text{THF}} [MgCl(THF)_5][FeMe_4] \xrightarrow[\text{-40 °C to RT}]{\text{THF}} S = 1/2\ (\text{EPR}) \quad (-CH_3CH_3)$$

$S = 3/2$

JACS
JOURNAL OF THE AMERICAN CHEMICAL SOCIETY

Communication

pubs.acs.org/JACS

Isolation, Characterization, and Reactivity of $Fe_8Me_{12}^-$: Kochi's $S = 1/2$ Species in Iron-Catalyzed Cross-Couplings with MeMgBr and Ferric Salts

Salvador B. Muñoz III, Stephanie L. Daifuku, William W. Brennessel, and Michael L. Neidig*

Department of Chemistry, University of Rochester, Rochester, New York 14627, United States

Supporting Information

Scheme 1. Spectroscopic Studies and Kochi's Mechanistic Proposal for Iron-Catalyzed Cross-Couplings with MeMgBr and Simple Ferric Salts

Kochi et al.

$FeCl_3 + CH_3MgBr \xrightarrow[\text{-40 °C to RT}\ \text{-}CH_3CH_3]{\text{THF}} S = 1/2\ \text{(EPR)}$

Neidig et. al.

$FeCl_3 + CH_3MgBr \xrightarrow[\text{-80 °C}]{\text{THF}} [MgCl(THF)_5][FeMe_4] \xrightarrow[\text{-40 °C to RT}\ \text{-}CH_3CH_3]{\text{THF}} S = 1/2\ \text{(EPR)}$

$S = 3/2$

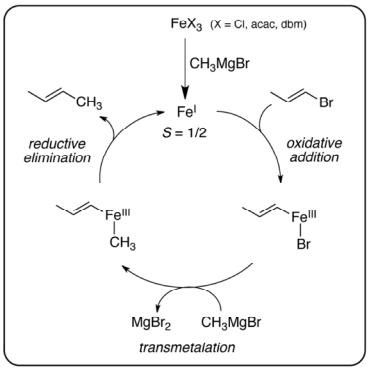

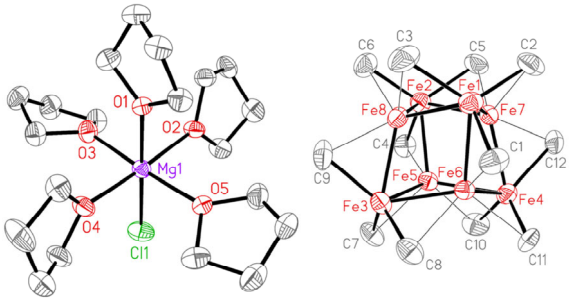

Figure 1. X-ray crystal structure of $[MgCl(THF)_5][Fe_8Me_{12}]$ (**1**) with selected

Scheme 2. Reactions of 1 with *β*-Bromostyrene

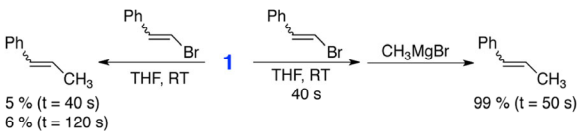

Cross-Coupling

International Edition: DOI: 10.1002/anie.201802087
German Edition: DOI: 10.1002/ange.201802087

The *N*-Methylpyrrolidone (NMP) Effect in Iron-Catalyzed Cross-Coupling with Simple Ferric Salts and MeMgBr

*Salvador B. Muñoz III[+], Stephanie L. Daifuku[+], Jeffrey D. Sears, Tessa M. Baker, Stephanie H. Carpenter, William W. Brennessel, and Michael L. Neidig**

Abstract: *The use of N-methylpyrrolidone (NMP) as a co-solvent in ferric salt catalyzed cross-coupling reactions is crucial for achieving the highly selective, preparative scale formation of cross-coupled product in reactions utilizing alkyl Grignard reagents. Despite the critical importance of NMP, the molecular level effect of NMP on in situ formed and reactive iron species that enables effective catalysis remains undefined. Herein, we report the isolation and characterization of a novel trimethyliron(II) ferrate species, $[Mg(NMP)_6][FeMe_3]_2$ (**1**), which forms as the major iron species in situ in reactions of $Fe(acac)_3$ and MeMgBr under catalytically relevant conditions where NMP is employed as a co-solvent. Importantly, combined GC analysis and ^{57}Fe Mössbauer spectroscopic studies identified **1** as a highly reactive iron species for the selective formation generating cross-coupled product. These studies demonstrate that NMP does not directly interact with iron as a ligand in catalysis but, alternatively, interacts with the magnesium cations to preferentially stabilize the formation of **1** over $[Fe_8Me_{12}]^-$ cluster generation, which occurs in the absence of NMP.*

Kochi 1971

Cahiez 1998

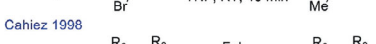

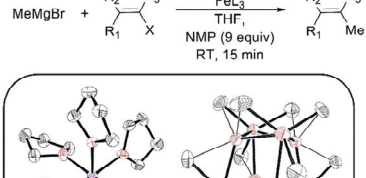

Angew. Chem. Int. Ed. **2018**, *57*, 6496.

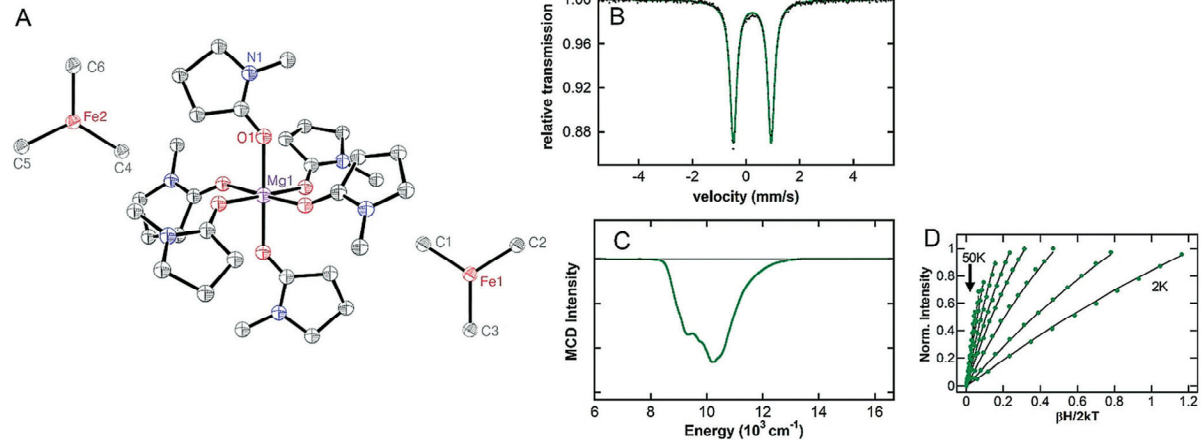

Figure 2. (A) Structure of $[Mg(NMP)_6][FeMe_3]_2$ (**1**), drawn at 50% probability level. Hydrogen atoms omitted for clarity. (B) 80 K ^{57}Fe Mössbauer spectrum of a frozen solution of **1** (black dots), total fit (green line). (C) 5 K, 7 T NIR MCD of **1** dissolved in 1:1 THF/2-MeTHF. (D) Saturation magnetization data (dots) and best fit (lines) collected at 10486 cm^{-1}.

Table 1: GC analysis of the products formed upon reaction of in situ generated **1** with β-bromostyrene at 23 °C

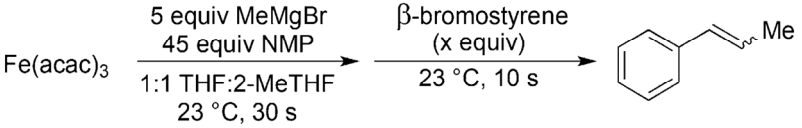

β-Bromostyrene [equiv]	Me-Styrene yield [%][a,b]
0.25	25
0.50	50
0.75	75

[a] Yields are with respect to iron. No other side products were observed. [b] Reactions are stereoselective and retain the same conformation in the cross-coupled product as in the starting reagent (*E*- and *Z*-isomers present). Yields account for both observed isomers.

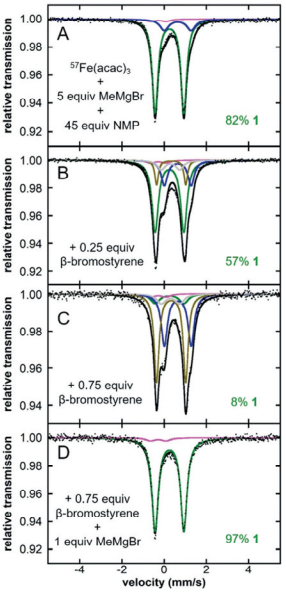

Cross-Coupling

International Edition: DOI: 10.1002/anie.201813578
German Edition: DOI: 10.1002/ange.201813578

The Effect of β-Hydrogen Atoms on Iron Speciation in Cross-Couplings with Simple Iron Salts and Alkyl Grignard Reagents

*Jeffrey D. Sears[+], Salvador B. Muñoz III[+], Stephanie L. Daifuku, Ari A. Shaps, Stephanie H. Carpenter, William W. Brennessel, and Michael L. Neidig**

Abstract: *The effects of β-hydrogen-containing alkyl Grignard reagents in simple ferric salt cross-couplings have been elucidated. The reaction of $FeCl_3$ with EtMgBr in THF leads to the formation of the cluster species $[Fe_8Et_{12}]^{2-}$, a rare example of a structurally characterized metal complex with bridging ethyl ligands. Analogous reactions in the presence of NMP, a key additive for effective cross-coupling with simple ferric salts and β-hydrogen-containing alkyl nucleophiles, result in the formation of $[FeEt_3]^-$. Reactivity studies demonstrate the effectiveness of $[FeEt_3]^-$ in rapidly and selectively forming the cross-coupled product upon reaction with electrophiles. The identification of iron-ate species with EtMgBr analogous to those previously observed with MeMgBr is a critical insight, indicating that analogous iron species can be operative in catalysis for these two classes of alkyl nucleophiles.*

Iron-catalyzed cross-coupling reactions of simple ferric salts and alkyl Grignard reagents have attracted significant interest since their initial development by Kochi in the 1970s.[1] Importantly, these reactions retain high fidelity even with the use of alkyl Grignard reagents containing β-hydrogen

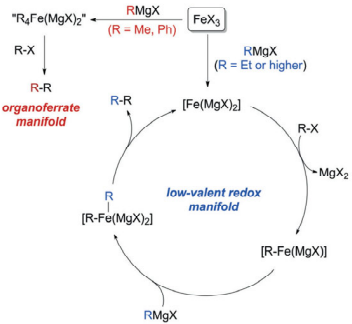

Scheme 1. Proposed divergent reactive iron species and mechanistic pathways for simple ferric salt cross-coupling with alkyl Grignard reagents with and without β-hydrogen atoms.

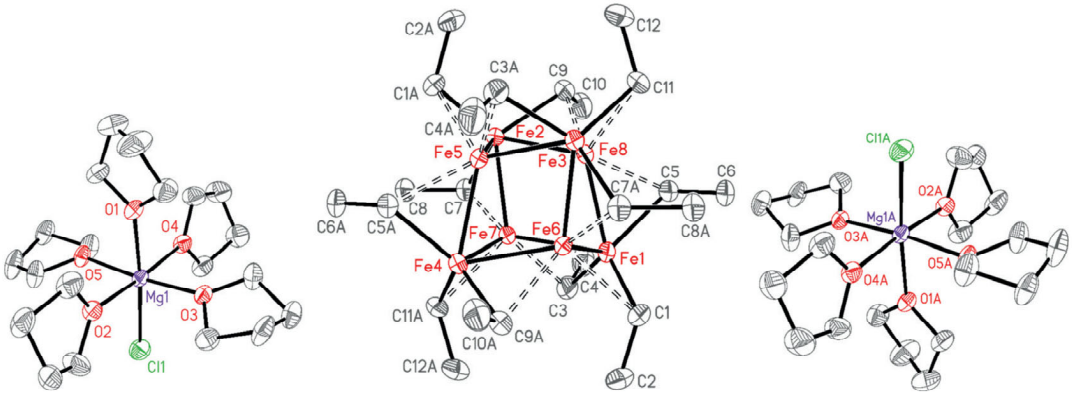

Figure 1. X-ray crystal structure of **1**. Anisotropic displacement ellipsoids drawn at the 50% probability level. The bridging ethyl ligands are common to both positions of the Fe_8 core, which is disordered over a crystallographic inversion center. Only one position of the Fe_8 core is shown, and hydrogen atoms and co-crystallized solvent molecules have been removed for clarity.

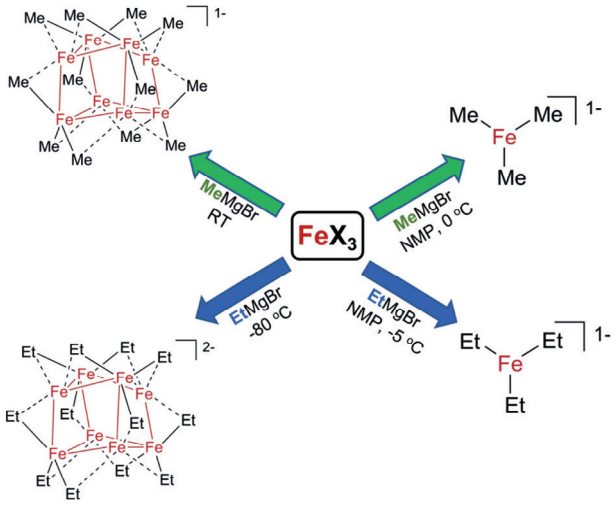

Scheme 2. Effect of β-hydrogen atoms on the structure of iron–alkyl species in reactions of simple ferric salts and alkyl Grignard reagents.

JACS
JOURNAL OF THE AMERICAN CHEMICAL SOCIETY
Article
Cite This: J. Am. Chem. Soc. 2019, 141, 10099−10108
pubs.acs.org/JACS

Mechanism of the Bis(imino)pyridine-Iron-Catalyzed Hydromagnesiation of Styrene Derivatives

Peter G. N. Neate,[‡,†] Mark D. Greenhalgh,[†] William W. Brennessel,[‡] Stephen P. Thomas,[‡,*] and Michael L. Neidig[*,‡]

[†]EaStCHEM School of Chemistry, University of Edinburgh, David Brewster Road, Edinburgh EH9 3FJ, U.K.
[‡]Department of Chemistry, University of Rochester, Rochester, New York 14627, United States

Supporting Information

ABSTRACT: Iron-catalyzed hydromagnesiation of styrene derivatives offers a rapid and efficient method to generate benzylic Grignard reagents, which can be applied in a range of transformations to provide products of formal hydrofunctionalization. While iron-catalyzed methodologies exist for the hydromagnesiation of terminal alkenes, internal alkynes, and styrene derivatives, the underlying mechanisms of catalysis remain largely undefined. To address this issue and determine the divergent reactivity from established cross-coupling and hydrofunctionalization reactions, a detailed study of the bis(imino)pyridine iron-catalyzed hydromagnesiation of styrene derivatives is reported. Using a combination of kinetic analysis, deuterium labeling, and reactivity studies as well as in situ ^{57}Fe Mössbauer spectroscopy, key mechanistic features and species were established. A formally iron(0) ate complex $[^{iPr}$BIPFe(Et)$(CH_2{=}CH_2)]^-$ was identified as the principle resting state of the catalyst. Dissociation of ethene forms the catalytically active species which can reversibly coordinate the styrene derivative and mediate a direct and reversible β-hydride transfer, negating the necessity of a discrete iron hydride intermediate. Finally, displacement of the tridentate bis(imino)pyridine ligand over the course of the reaction results in the formation of a tris-styrene coordinated iron(0) complex, which is also a competent catalyst for hydromagnesiation.

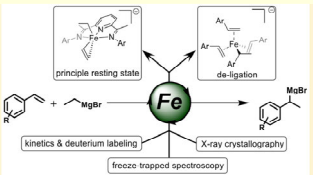

J. Am. Chem. Soc. **2019**, *141*, 10099.

Scheme 1. Iron-Catalyzed Hydromagnesiation of Alkylalkenes, Arylalkenes, and Alkynes

Shirakawa & Hayashi

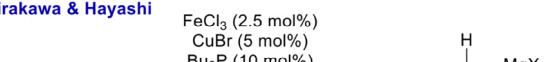

Thomas

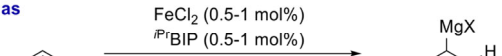

Nakamura

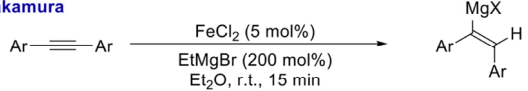

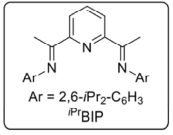

Scheme 2. Hydromagnesiation of 2-Methoxystyrene Using Different Grignard Reagents

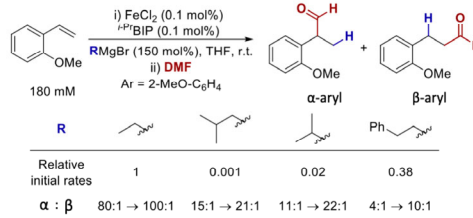

Scheme 3. Hydromagnesiation of 2-Methoxystyrene Using Deuterated Grignard Reagents

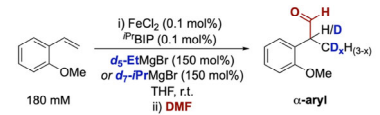

Scheme 4. Possible Mechanisms for the Iron-Catalyzed Isomerization of (2-Phenylethyl)magnesium Bromide

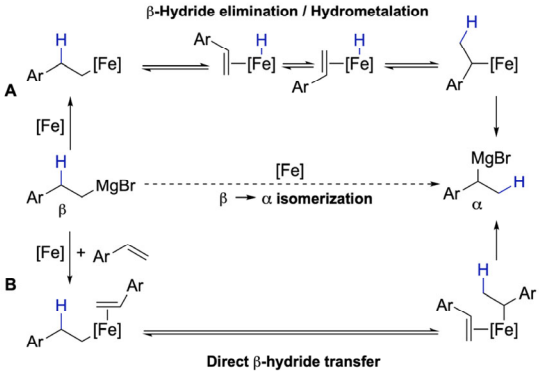

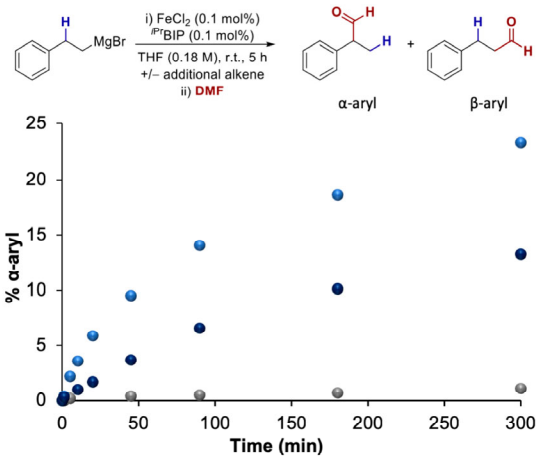

Figure 1. Isomerization of (2-phenylethyl)magnesium bromide. gray ● = no alkene added (0.5 mol % styrene present in Grignard reagent); light blue ● = styrene (10 mol %) added; dark blue ● = 1-octene (100 mol %) added.

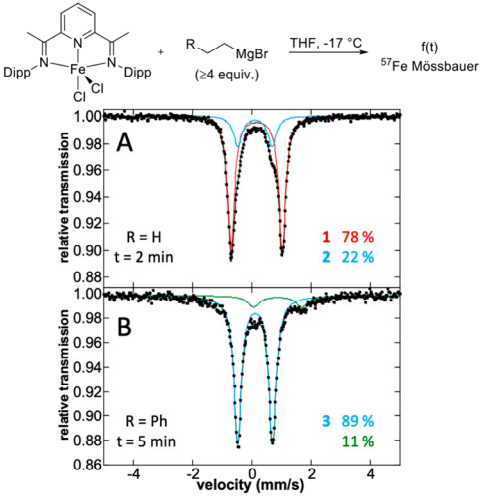

Figure 2. 80 K frozen solution Mössbauer spectrum of the reaction of ^{iPr}BIP^{52}FeCl$_2$ with (A) 4 equiv of EtMgBr for 2 min and (B) 10 equiv of Ph(CH$_2$)$_2$MgBr for 5 min.

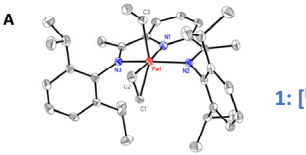

1: [^{iPr}BIPFe(Et)(CH$_2$=CH$_2$)][MgX(THF)$_5$]

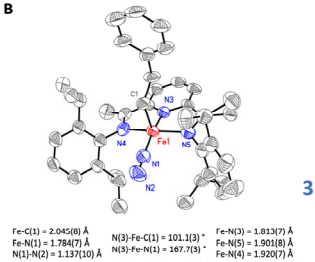

3: [^{iPr}BIPFe(PhCH$_2$CH$_2$)][MgX(THF)$_5$]

Figure 3. X-ray crystal structures of (A) [^{iPr}BIPFe(Et)(CH$_2$=CH$_2$)][MgX(THF)$_5$] **1** and (B) [^{iPr}BIPFe(N$_2$)(CH$_2$CH$_2$Ph)][MgX(THF)$_5$] **3**. Structures drawn with thermal displacement ellipsoids at 50% probability level. Iron shown in red; nitrogen atoms in blue; carbon in gray. Hydrogen atoms omitted for clarity. Note: magnesium countercation omitted for clarity.

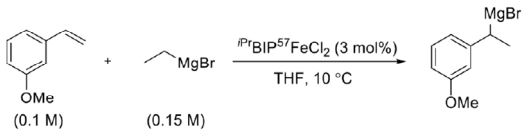

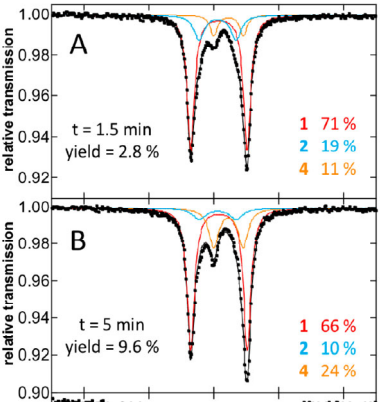

1: [^{iPr}BIPFe(Et)(CH_2=CH_2)][MgX($THF)_5$]

2:[^{iPr}BIPFe(N_2)(Et)(CH_2=CH_2)][MgX($THF)_5$]

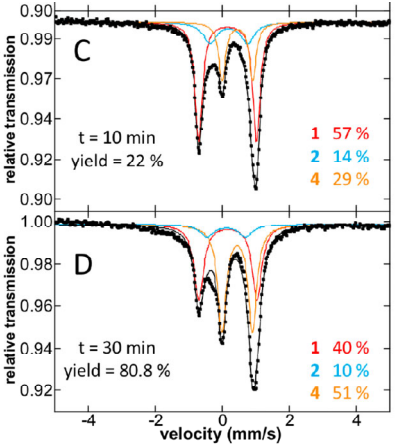

Figure 4. 80 K frozen solution Mössbauer spectra taken during hydromagnesiation of 3-methoxystyrene.

3: [^{iPr}BIPFe(PhCH$_2$CH$_2$)][MgX(THF)$_5$]

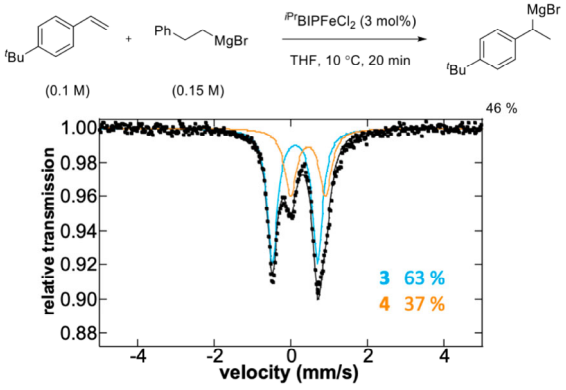

Figure 5. 80 K frozen solution Mössbauer spectrum taken 20 min into the hydromagnesiation reaction of 4-*tert*-butylstyrene using Ph-$(CH_2)_2$MgBr.

缺电子苯乙烯更有利于稳定中间体

4: [Fe(η^2-styrene)$_3$(κ^1–CH(CH$_3$)-Ph)][MgX(THF)$_5$]

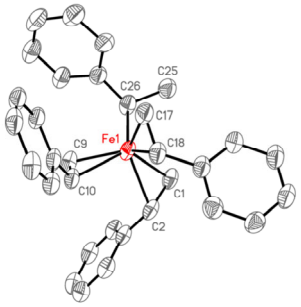

Fe-C(1) = 2.065(2) Å	C(26)-Fe-C(1) = 90.29(16) °	Fe-C(26) = 2.150(4) Å
Fe-C(2) = 2.209(2) Å	C(26)-Fe-C(2) = 123.23(16) °	C(25)-C(26) = 1.521(6) Å
Fe-C(17) = 2.056(3) Å	C(26)-Fe-C(17) = 95.22(18) °	C(1)-C(2) = 1.403(4) Å
Fe-C(18) = 2.233(3) Å	C(26)-Fe-C(18) = 129.27(17) °	C(17)-C(18) = 1.398(4) Å

Figure 6. X-ray crystal structure of [Fe(η^2-styrene)$_3$(κ^1–CH(CH$_3$)-Ph)][MgX(THF)$_5$] **4** and representative bond distances and angles. Structure drawn with thermal displacement ellipsoids at 50% probability level. Iron shown in red, carbon in gray. Hydrogen atoms omitted for clarity. Note: magnesium countercation omitted for clarity.

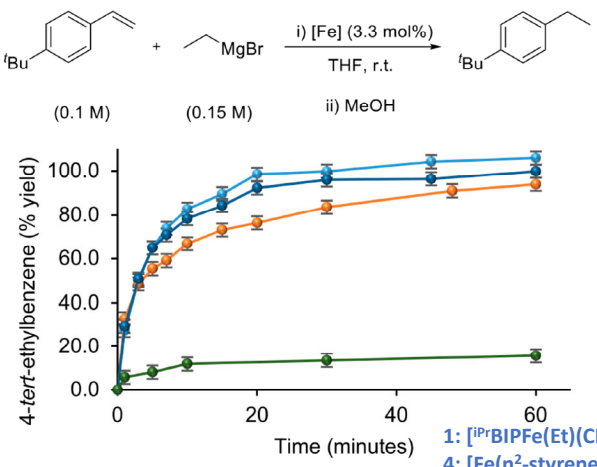

Figure 7. Hydromagnesiation of 4-*tert*-butylstyrene using isolated iron sources. light blue ● = complex **1**; dark blue ● = ^{iPr}BIPFeCl$_2$; orange ● = complex **4**; green ● = FeCl$_2$.

Scheme 5. Proposed Catalytic Cycle for the BIPFe-Catalyzed Hydromagnesiation of Styrene Derivatives

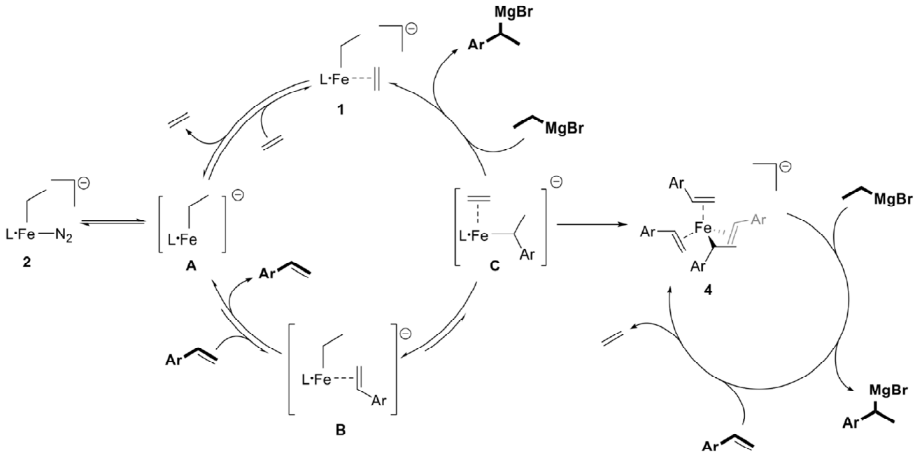

Catalysis

How to cite: *Angew. Chem. Int. Ed.* **2020**, *59*, 17070–17076
International Edition: doi.org/10.1002/anie.202006639
German Edition: doi.org/10.1002/ange.202006639

TMEDA in Iron-Catalyzed Hydromagnesiation: Formation of Iron(II)-Alkyl Species for Controlled Reduction to Alkene-Stabilized Iron(0)

Peter G. N. Neate, Mark D. Greenhalgh, William W. Brennessel, Stephen P. Thomas, and Michael L. Neidig**

Abstract: *N,N,N′,N′-Tetramethylethylenediamine (TMEDA) has been one of the most prevalent and successful additives used in iron catalysis, finding application in reactions as diverse as cross-coupling, C–H activation, and borylation. However, the role that TMEDA plays in these reactions remains largely undefined. Herein, studying the iron-catalyzed hydromagnesiation of styrene derivatives using TMEDA has provided molecular-level insight into the role of TMEDA in achieving effective catalysis. The key is the initial formation of TMEDA–iron(II)–alkyl species which undergo a controlled reduction to selectively form catalytically active styrene-stabilized iron(0)–alkyl complexes. While TMEDA is not bound to the catalytically active species, these active iron(0) complexes cannot be accessed in the absence of TMEDA. This mode of action, allowing for controlled reduction and access to iron(0) species, represents a new paradigm for the role of this important reaction additive in iron catalysis.*

pling of aryl bromides with alkyl or alkenyl halides;[17,18] difluoroalkylation;[77] and release-capture ethylene coupling.[21] Additionally, the use of TMEDA as an additive extends well beyond cross-coupling, having proved essential for reactions including Miyaura-type borylation of alkyl electrophiles, C–H alkylation and the hydromagnesiation of styrene derivatives (Scheme 1 B–D).[23–27]

Despite being a crucial component of many reactions, the role that TMEDA plays in achieving effective catalysis within such reactions is largely undefined. Attempts to ascertain its function within iron-catalyzed cross-coupling reactions have been a particular focus, with Bedford and co-workers having carried out perhaps the most extensive investigations.[28–31] However, a definitive role has yet to be established. Early work by Nagashima and co-workers suggested that TMEDA coordinates the iron center, with productive reactivity taking place from the bis-transmetallated complex.[28] Bedford and co-workers later showed that this TMEDA-bound species did

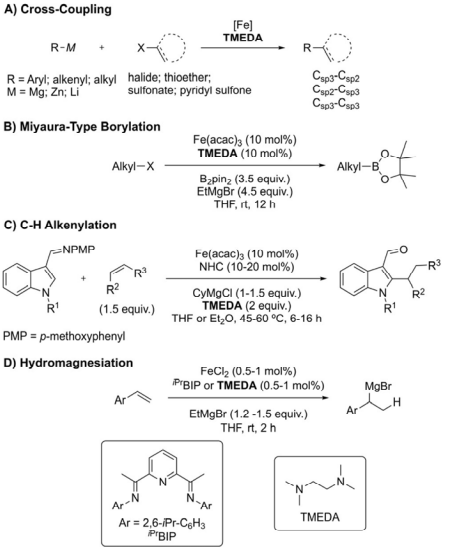

Scheme 1. Examples of iron-catalyzed reactions that use TMEDA as an additive.

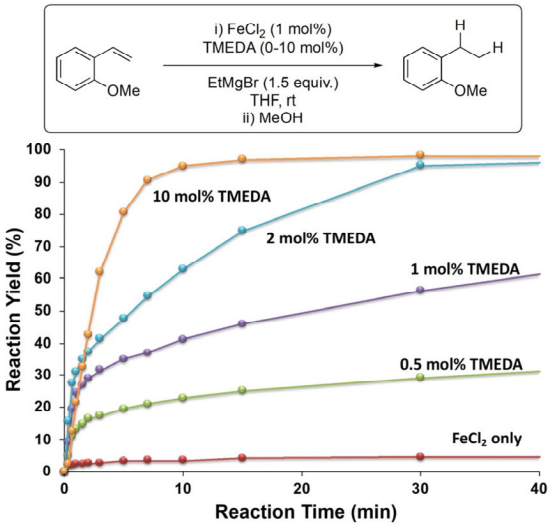

Figure 1. Kinetic profile of the hydromagnesiation of 2-methoxystyrene with various equivalents of TMEDA.

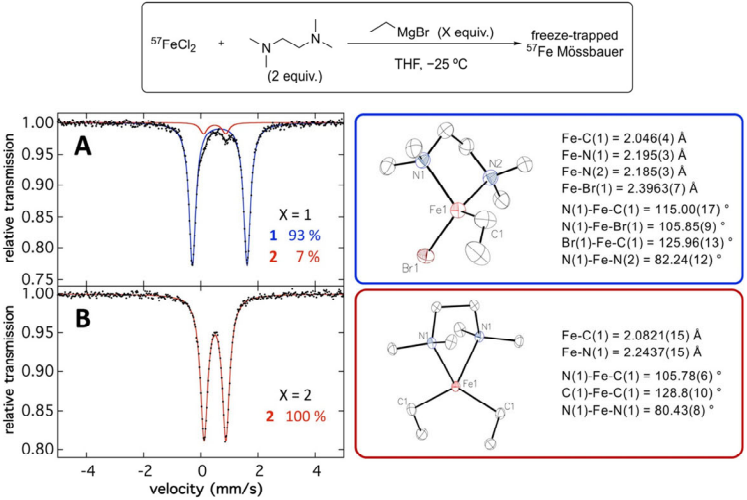

Figure 2. 80 K frozen solution Mössbauer spectra of the reaction of $^{57}FeCl_2$ with EtMgBr in the presence of 2 equiv TMEDA and X-Ray crystal structures of major species formed with representative bond distances and angles. A) 1 equiv EtMgBr, structure displays a halogen disorder with 70% bromide and 30% chloride occupancies. B) 2 equiv EtMgBr. Note: Structure drawn with thermal displacement ellipsoids at 50% probability level. Iron shown in red, carbon in grey, and hydrogen atoms omitted for clarity.

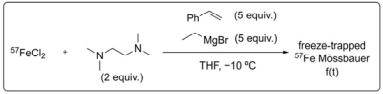

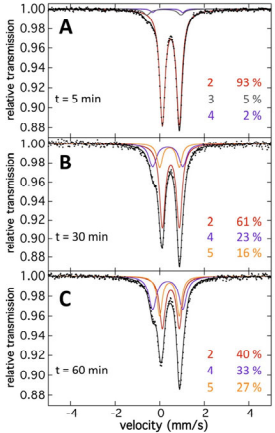

2: (TMEDA)$FeEt_2$
3: $[Fe_8Et_{12}][MgX(THF)_5]_2$
4: $(styrene)_3Fe^0$-Et
5: $(styrene)_3Fe^0$-a-aryl

Figure 3. 80 K frozen-solution Mössbauer spectra of the reaction of $^{57}FeCl_2$ and 2 equiv TMEDA with EtMgBr (5 equiv) and styrene (5 equiv) for A) 5 minutes; B) 30 minutes; C) 60 minutes.

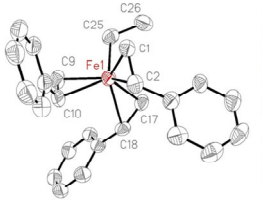

Figure 4. X-Ray crystal structure of [Fe(η²-styrene)₃(Et)][MgX(THF)₅] **4** with representative bond distances and angles. Note: magnesium counter-cation omitted for clarity. Structure drawn with thermal displacement ellipsoids at 50% probability level. Iron shown in red, carbon in grey, nitrogen in blue and hydrogen atoms omitted for clarity.

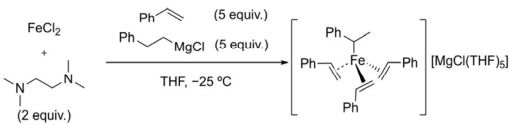

5

Scheme 2. Formation of **5** from the reaction of $FeCl_2$ with Ph-$(CH_2)_2$MgCl in the presence of styrene and TMEDA.

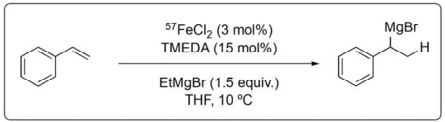

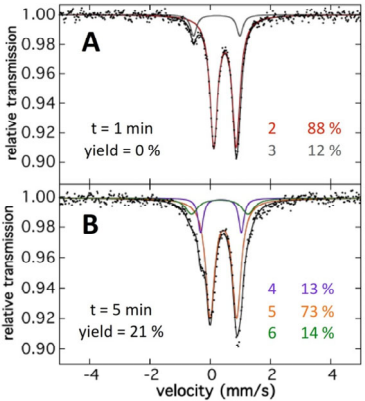

Figure 5. 80 K frozen solution Mössbauer spectra taken as a function of time during catalytic hydromagnesiation of styrene.

2: (TMEDA)$FeEt_2$
3: $[Fe_8Et_{12}][MgX(THF)_5]_2$
4: $(styrene)_3Fe^0$-Et
5: $(styrene)_3Fe^0$-a-aryl
6可能是配有多个苯乙烯的0价铁络合物

TMEDA的作用

1、TMEDA通过抑制铁(0)络合物的聚集防止催化剂失活。
2、TMEDA影响铁(II)络合物的还原。
3、TMEDA虽然不与关键中间体络合，但是是反应所必需的。

VIP Catalysis Very Important Paper

How to cite: *Angew. Chem. Int. Ed.* **2022,** *61,* e202114986
International Edition: doi.org/10.1002/anie.202114986
German Edition: doi.org/10.1002/ange.202114986

A TMEDA–Iron Adduct Reaction Manifold in Iron-Catalyzed C(sp^2)–C(sp^3) Cross-Coupling Reactions

*Nikki J. Bakas[+], Jeffrey D. Sears[+], William W. Brennessel, and Michael L. Neidig**

Abstract: Herein, we expand the current molecular-level understanding of one of the most important and effective additives in iron-catalyzed cross-coupling reactions, *N*,*N*,*N*′,*N*′-tetramethylethylenediamine (TMEDA). Focusing on relevant phenyl and ethyl Grignard reagents and slow nucleophile addition protocols commonly used in effective catalytic systems, TMEDA-iron(II)-aryl intermediates are identified via in situ spectroscopy, X-ray crystallography, and detailed reaction studies to be a part of an iron(II)/(III)/(I) reaction cycle where radical recombination with FePhBr(TMEDA) ($\mathbf{2_{Ph}}$) results in selective product formation in high yield. These results differ from prior studies with mesityl Grignard reagent, where poor product selectivity and low catalytic performance can be attributed to homoleptic iron–ate species. Overall, this study represents a critical advance in how amine additives such as TMEDA can modulate selectivity and reactivity of organoiron species in cross-coupling.

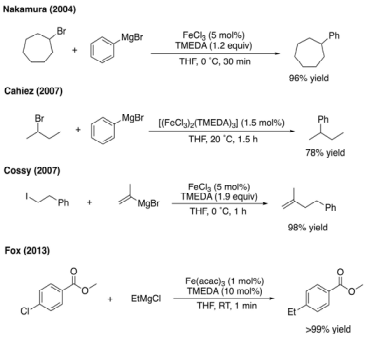

Scheme 1. Representative examples of iron-catalyzed Kumada cross-coupling reactions using TMEDA.

2_{Ph}: FePhBr(TMEDA)
3_{Ph}: $FePh_2$(TMEDA)

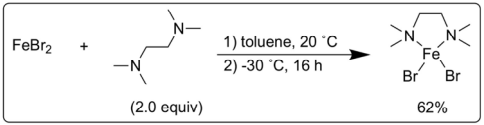

Fe-N(1)	2.1428(19)	Å
Fe-N(2)	2.1788(19)	Å
Fe-Br(2)	2.3817(6)	Å
Fe-Br(1)	2.3983(6)	Å

N(1)-Fe-N(2)	83.13(7)°
N(1)-Fe-Br(2)	113.32(5)°
Br(2)-Fe-Br(1)	122.445(17)°
C(1)-N(1)-Fe	113.61(15)°

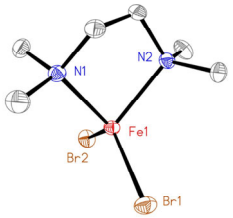

Figure 1. Synthesis of $FeBr_2$(TMEDA) (**1**). Crystal structure of **1** with selected bond lengths and angles. Note: Hydrogen atoms omitted for clarity and ellipsoids drawn at 50% probability level.

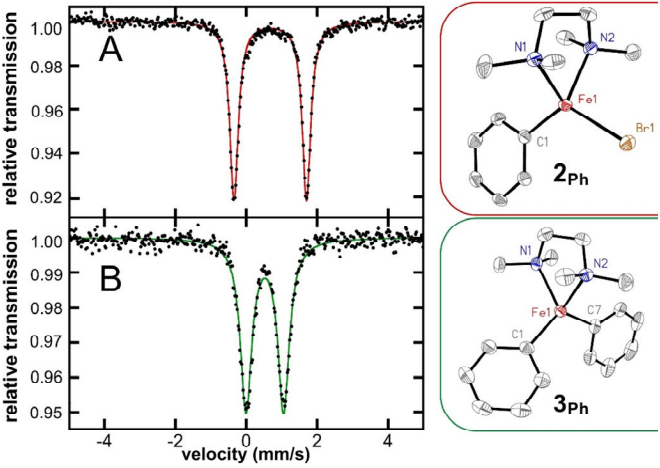

Figure 2. 80 K Mössbauer spectra of in situ generated A) FePhBr(TMEDA) (2_{Ph}) with $\delta = 0.68$ mm s^{-1} and $FePh_2$(TMEDA) (3_{Ph}) with $\delta = 0.52$ mm s^{-1} and $|\Delta E_Q| = 1.06$ mm s^{-1}. Crystal structures and bond metrics Hydrogen atoms omitted for clarity and ellipsoids drawn at 50% probability level.

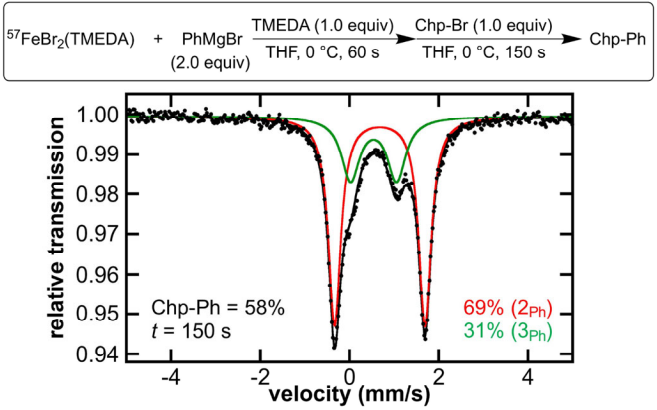

Figure 3. 80 K Mössbauer spectra of frozen solution of reaction of in situ generated $FePh_2(TMEDA)$ (**3_{Ph}**) with 1.0 equiv of Chp-Br after 150 s; raw data (black dots), total fit (black trace), individual fit components are shown.

2_{Ph}: FePhBr(TMEDA)
3_{Ph}: $FePh_2$(TMEDA)

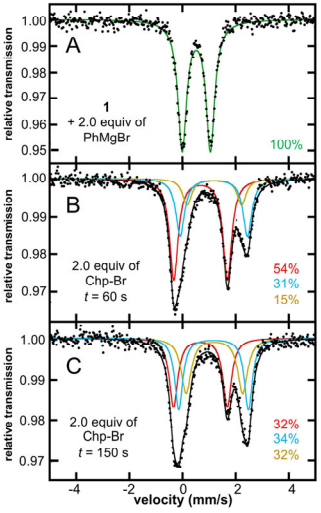

Figure 4. 80 K Mössbauer spectra of frozen solution time points of A) in situ generated $FePh_2(TMEDA)$ (**3_{Ph}**) and reaction of 2.0 equiv of Chp-Br after B) 60 s and C) 150 s; raw data (black dots), total fit (black trace), individual fit components are shown.

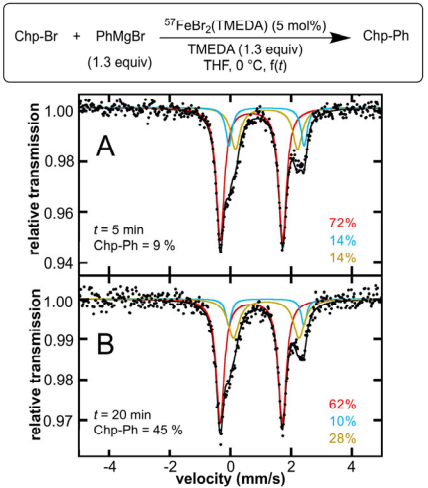

Figure 5. Freeze-trapped 80 K Mössbauer spectrum of the iron speciation in the iron-catalyzed cross-coupling of PhMgBr and Chp-Br at A) 5 min and B) 20 min; raw data (black dots), total fit (black trace), individual fit components are shown.

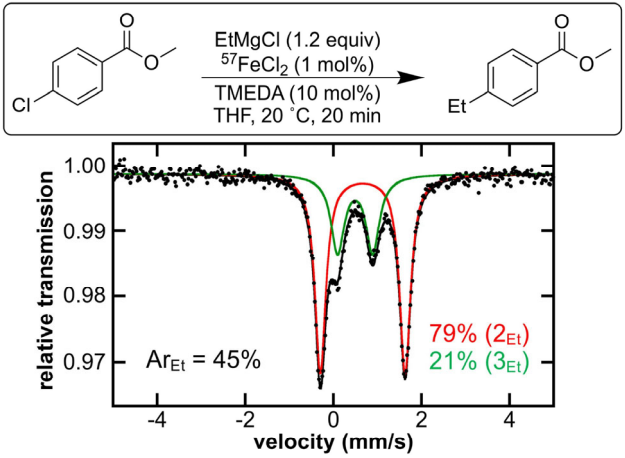

Figure 6. Freeze-trapped 80 K Mössbauer spectrum of Fox catalysis at 20 min (ca. halfway through catalysis); raw data (black dots), total fit (black trace), individual fit components are shown.

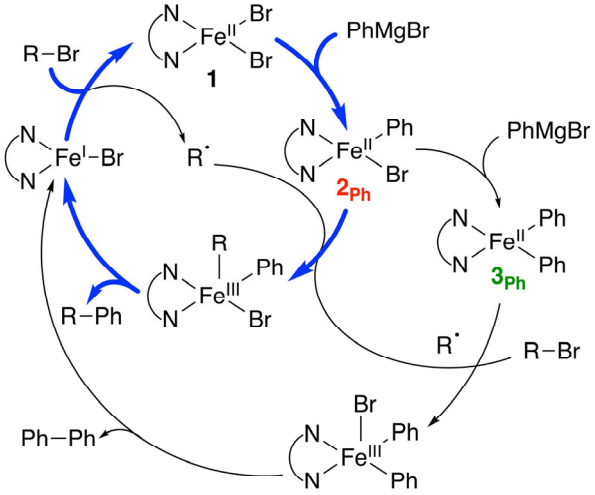

Scheme 2. Proposed mechanism of iron-catalyzed C(sp^2)–C(sp^3) cross-coupling using TMEDA and phenyl Grignard reagent, main cycle is guided by bolded blue arrows.

GDCh Communication Angewandte International Edition Chemie www.angewandte.org

How to cite: *Angew. Chem. Int. Ed.* **2024**, *63*, e202405113
doi.org/10.1002/anie.202405113

Coordination Chemistry Hot Paper

Unusual $S = 1$ Four-Coordinate Fe(IV) Complexes Supported by Bisamide Ligands: Syntheses, Characterization, and Electronic Structures

*Bufan Zhang, Justin P. Joyce, Nikki J. Wolford, William W. Brennessel, Serena DeBeer, and Michael L. Neidig**

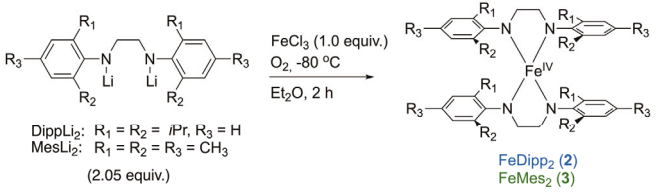

Scheme 1. Syntheses of **2** and **3** via one-pot in situ oxidation of their respective ferric precursors with O_2.

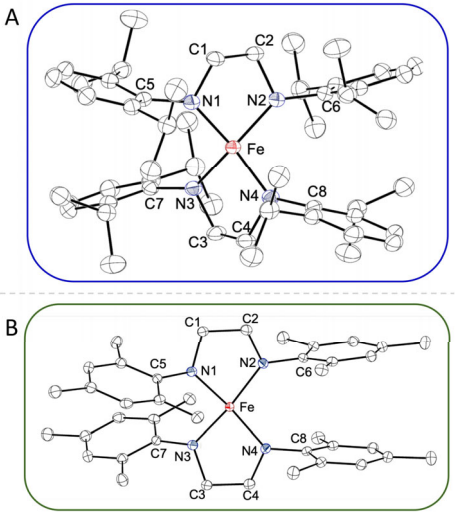

ORGANIC CHEMISTRY

General method for iron-catalyzed multicomponent radical cascades–cross-couplings

Lei Liu[1]†, Maria Camila Aguilera[2]†, Wes Lee[1], Cassandra R. Youshaw[1], Michael L. Neidig[2]*, Osvaldo Gutierrez[1,3]*

Transition metal–catalyzed cross-coupling reactions are some of the most widely used methods in chemical synthesis. However, despite notable advantages of iron (Fe) as a potentially cheaper, more abundant, and less toxic transition metal catalyst, its practical application in multicomponent cross-couplings remains largely unsuccessful. We demonstrate 1,2-bis(dicyclohexylphosphino)ethane Fe–catalyzed coupling of α-boryl radicals (generated from selective radical addition to vinyl boronates) with Grignard reagents. Then, we extended the scope of these radical cascades by developing a general and broadly applicable Fe-catalyzed multicomponent annulation–cross-coupling protocol that engages a wide range of π-systems and permits the practical synthesis of cyclic fluorous compounds. Mechanistic studies are consistent with a bisarylated Fe(II) species being responsible for alkyl radical generation to initiate catalysis, while carbon-carbon bond formation proceeds between a monoarylated Fe(II) center and a transient alkyl radical.

Science, **2021**, *374*, 432.

A **Fe-catalyzed cross-coupling of C-center radicals**

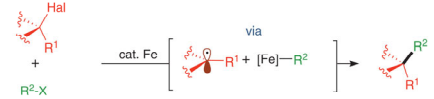

Partner 1: Hal = I, Br, Cl
Partner 2: X = [Mg], [Zn], etc.

R^1 = alkyl, aryl, alkoxy, ester (well-established)
= boryl (**not known**)

B **Strategies for multicomponent transition metal-catalyzed cross-coupling of α-boryl radicals**

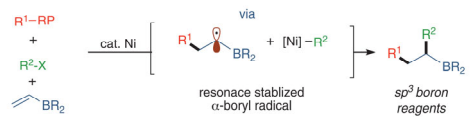

Partner 1: RP = I, Br, BF_3K, CO_2H, $Si(cat)_2$
Partner 2: X = I, Br, [Zn]
Partner 3: vinyl boronates

C **Fe-catalyzed multicomponent radical cascade–cross-couplings (this work)**

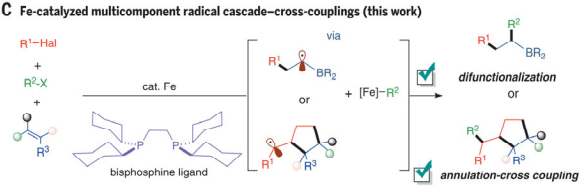

Partner 1: Hal = I and Br
Partner 2: X = [Mg]
Partner 3: R^3 = BR_2, OR, SR, SiR_3, NR_2, and alkyl

Fig. 1. Metal-catalyzed cross-coupling of α-boryl radicals. (**A**) Established methods for Fe-catalyzed C–C cross-coupling with alkyl radicals. (**B**) Current strategies for three-component trapping of α-boryl radicals. (**C**) Our report on the use of bisphosphine-iron complexes to promote radical cascade–cross-coupling reactions.

Kumada Three-Component Cross-Coupling

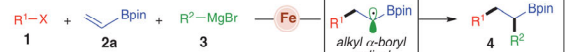

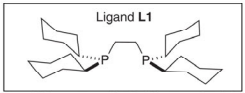

Conditions: 10 mol% $FeCl_3$, 20 mol% **L1**, THF, 0 °C, 1 h

Variation of the nucleophile (R^2)

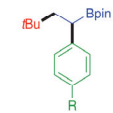

X = Br

R = H, **4a**, 75%
OMe, **4b**, 64%
Ph, **4c**, 73%
Me, **4d**, 71%
Cl, **4e**, 84%
F, **4f**, 69%

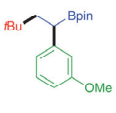

4g, X = Br, 74%
4h, X = I, 83%

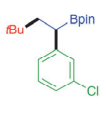

4i, X = I, 76%

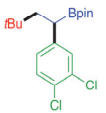

4j, X = Br, 61%

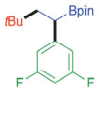

4k, X = Br, 81%

4l, X = Br, 84%

4m, X = Br, 66%

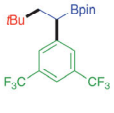

4n, X = Br, 63%
4o, X = I, 71%

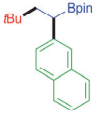

4p, X = Br, 63%
4q, X = I, 80%

4r, X = I, 53%

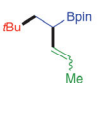

4s, X = I, 42%

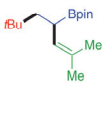

4t, X = Br, 47%
4u, X = I, 56%

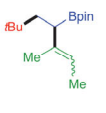

4v, X = I, 40%

notable limitations

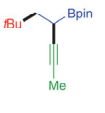

4w, X = I, 30%
4x, X = Br, < 5%

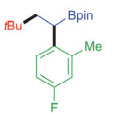

4y, X = I, < 5%

Variation of the alkyl halide (R^1)

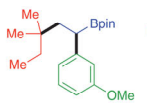

4a', X = Br, 64%

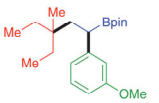

4b', X = Br, 57%

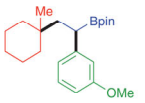

4c', X = Br, 83%

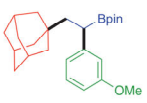

4d', X = Br, 30%
4e', X = I, 70%

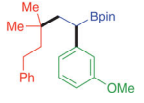

4f', X = Br, 60%

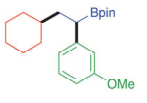

4g', X = I, 39%*

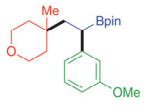

4h', X = Br, 89%

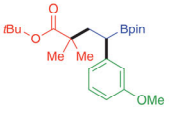

4i', X = Br, 40%*

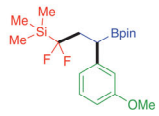

4j', X = Br, 62%

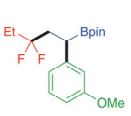

4k', X = Br, 39%

4l', X = Br, 65%

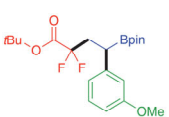

4m', X = Br, 36%

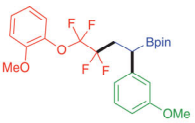

4n', X = Br, 81%

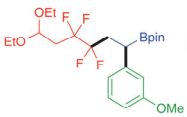

4o', X = Br, 61%

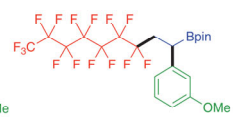

4p', X = Br, 56%

notable limitations

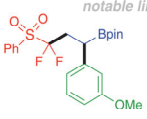

4q', X = Br, < 5%

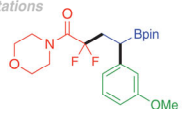

4r', X = Br, < 5%

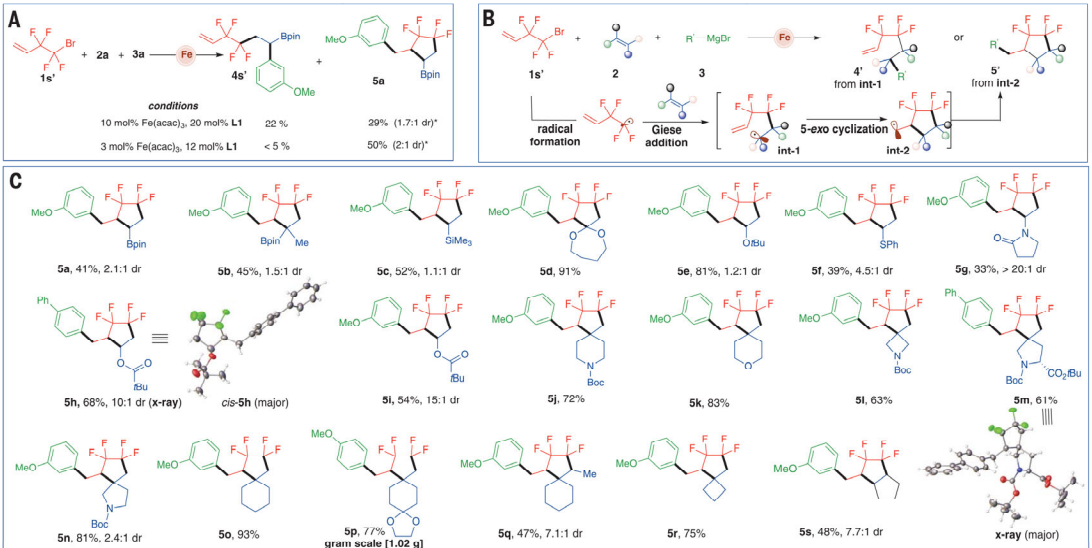
A
1s'
2a
3a
Fe
4s'
Bpin
OMe
5a
conditions
10 mol% Fe(acac)3, 20 mol% L1 22 % 29% (1.7:1 dr)*
3 mol% Fe(acac)3, 12 mol% L1 < 5 % 50% (2:1 dr)*
B
1s'
2
R' MgDr
Fe
3
4' from int-1
or
5' from int-2
radical formation
Giese addition
int-1
5-exo cyclization
int-2
C
5a, 41%, 2.1:1 dr
5b, 45%, 1.5:1 dr
5c, 52%, 1.1:1 dr
5d, 91%
5e, 81%, 1.2:1 dr
5f, 39%, 4.5:1 dr
5g, 33%, > 20:1 dr
5h, 68%, 10:1 dr (x-ray)
cis-5h (major)
5i, 54%, 15:1 dr
5j, 72%
5k, 83%
5l, 63%
5m, 61%
5n, 81%, 2.4:1 dr
5o, 93%
5p, 77%
gram scale [1.02 g]
5q, 47%, 7.1:1 dr
5r, 75%
5s, 48%, 7.7:1 dr
x-ray (major)

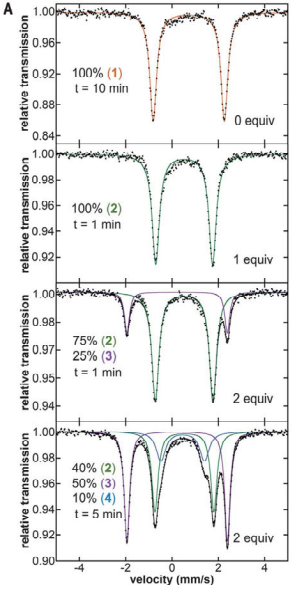

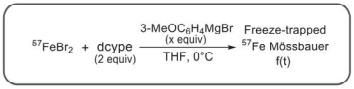

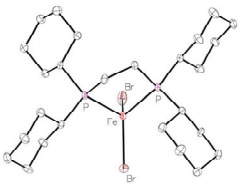

Fe(dcype)Br_2 (**1**)

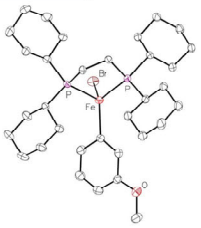

Fe(dcype)Br(3-$MeOC_6H_4$) (**2**)

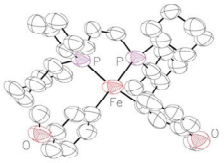

Fe(dcype)(3-$MeOC_6H_4$)$_2$ (**3**)

(dcype)Fe(η^6-(3,3'-$(OMe)_2$-1,1'-$(C_6H_4)_2$)) (**4**)

B

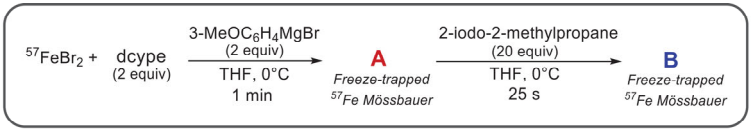

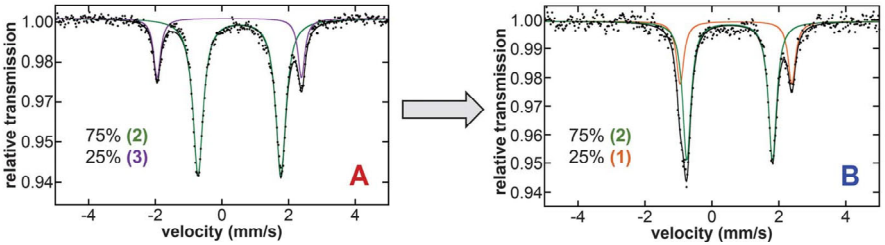

Fig. 4. Freeze-trapped 80 K Mössbauer spectra of stoichiometric reactions. (**A**) $^{57}FeBr_2$, 2 equiv of **L1**, and various equivalents of 3-MeOC$_6$H$_4$MgBr (left). Combining SC-XRD and Mössbauer studies of crystalline material, the individual components were assigned as Fe(dcype)Br$_2$ (**1**) (orange), Fe(dcype)Br(3-MeOC$_4$H$_6$) (**2**) (green), Fe(dcype)(3-MeOC$_4$H$_6$)$_2$ (**3**) (purple), and (dcype)Fe{η^6-[3,3′-(OMe)$_2$-1,1′-(C$_4$H$_6$)$_2$]} (**4**) (blue). Thermal ellipsoids are shown at 50% probability. (**B**) The freeze-trapped 80 K Mössbauer spectrum of the in situ formed iron species upon reaction of $^{57}FeBr_2$ and 2 equiv of **L1**, with 2 equiv of 3-MeOC$_6$H$_4$MgBr for 1 min (left) and following subsequent reaction with 2-iodo-2-methylpropane for 25 s (right).

A Intermediacy of alkyl radical

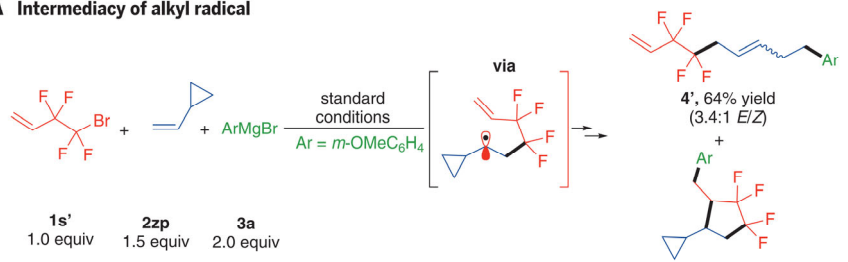

B Stereoconvergence via alkyl radical C-C bond rotation

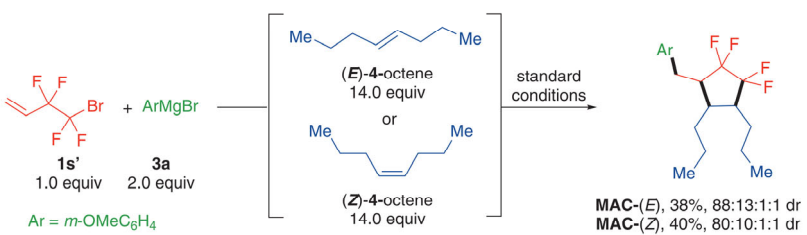

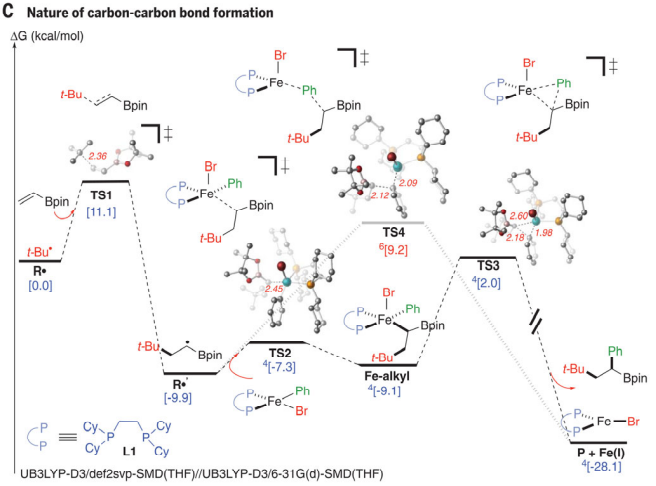

Fig. 5. Experimental and DFT calculations insights into the mechanism. (**A** and **B**) Standard conditions were carried out on a 0.20-mmol scale at 0°C; Grignard reagent **3a** was added dropwise by means of a syringe pump over 1 hour. Reported yields and dr are from isolated yields. (**C**) Computed lowest-energy pathway for the Fe-catalyzed multicomponent radical cascade cross-coupling reaction leading to dicarbofunctionalization of vinyl boronates. TS, transition state structure.

nature communications

Article

https://doi.org/10.1038/s41467-024-47589-7

Iron-catalyzed stereoselective C–H alkylation for simultaneous construction of C–N axial and *C*-central chirality

Received: 5 June 2023

Accepted: 4 April 2024

Published online: 25 April 2024

Zi-Jing Zhang[1], Nicolas Jacob[2], Shilpa Bhatia[3], Philipp Boos[1], Xinran Chen[1,4], Joshua C. DeMuth[3], Antonis M. Messinis[1], Becky Bongsuiru Jei[1], João C. A. Oliveira[1], Aleksa Radović[3], Michael L. Neidig[5] ✉, Joanna Wencel-Delord[2,6] ✉ & Lutz Ackermann[1,7] ✉

a Fe as catalyst of choice for catalytic transformations

Natural abundance of common transition metals in Earth's crust

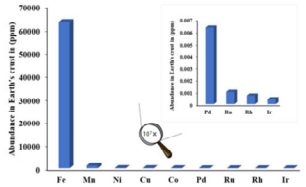

b Different approaches for iron-catalyzed asymmetric transformation

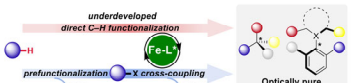

Chiral ligands used in iron catalyzed enantioselective cross couplings

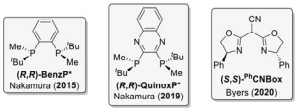

c Iron-catalyzed enantioselective C–H alkylation

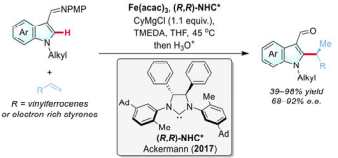

d Examples of bioactive C-N axially chiral compounds

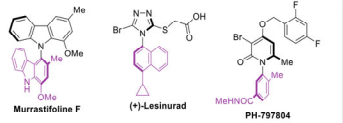

e This work

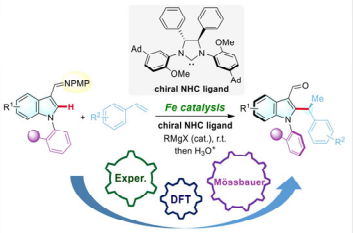

- ♦ *Fe-catalyzed stereoselective C–H alkylation*
- ♦ *Simultaneous construction of axial chirality and central chirality*
- ♦ *Generation of rare C-N axially chiral indoles*
- ♦ *Mild reaction conditions* ♦ *Detailed DFT calculations*
- ♦ *Catalytic active iron(0) species (detected by Mössbauer spectroscopy)*

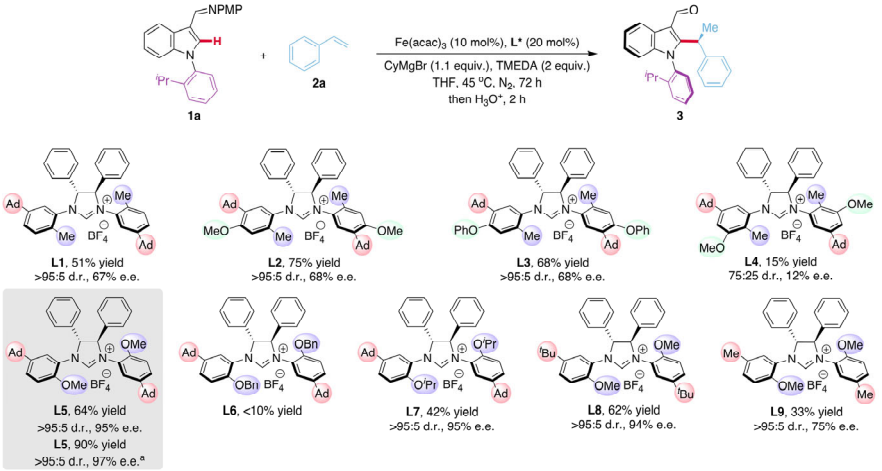

Fig. 2 | Condition optimization for the iron-catalyzed asymmetric C–H alkylation. Reaction conditions: **1a** (0.1 mmol), **2a** (0.15 mmol), $Fe(acac)_3$ (10 mol%), **L*** (20 mol%), CyMgBr (1 M in THF, 0.11 mmol) and TMEDA (0.2 mmol) were stirred in THF (0.2 mL) at 45 °C for 72 h under N_2, then added HCl aq. (1 M, 1.0 mL) and stirred for 2 h. The yield was determined by ^1H NMR spectroscopy using 1,3,5-trimethoxybenzene as the internal standard. The diastereomeric ratio (d.r.) was determined by ^1H NMR spectroscopy. The enantiomeric excess (e.e.) was determined by HPLC. [a]**1a** (0.1 mmol), **2a** (0.15 mmol), $Fe(acac)_3$ (10 mol%), **L5** (10 mol%), CyMgBr (1 M in THF, 50 mol%) and TMEDA (0.2 mmol) were stirred in Et_2O (0.2 mL) at room temperature for 72 h under N_2. TMEDA, *N,N,N′,N′*-tetramethylethylenediamine; THF, tetrahydrofuran.

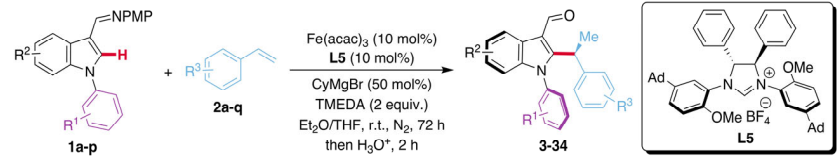

a Scope of *N*-substituents

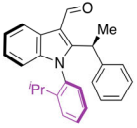

3, 90% yield
>95:5 d.r., 97% e.e.

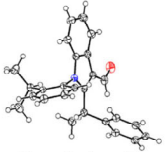

X-ray structure of **3**

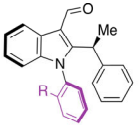

4, R = Me, 91% yield, >95:5 d.r., 95% e.e.
5, R = Et, 91% yield, >95:5 d.r., 97% e.e.
6, R = Ph, 73% yield, >95:5 d.r., 98% e.e.
7, R = OCF_3, 68% yield, >95:5 d.r., 91% e.e.
8, R = Cl, 56% yield, >95:5 d.r., 94% e.e.

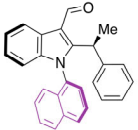

9, 86% yield
>95:5 d.r., 93% e.e.

b Scope of indoles

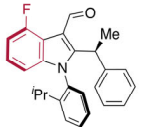

10, 36% yield
90:10 d.r., 90% e.e.

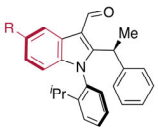

11, R = F, 63% yield, >95:5 d.r., 94% e.e.
12, R = Me, 82% yield, >95:5 d.r., 96% e.e.
13, R = OMe, 70% yield, >95:5 d.r., 98% e.e.
14, R = OBn, 54% yield, >95:5 d.r., 98% e.e.

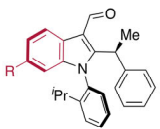

15, R = Cl, 50% yield, >95:5 d.r., 87% e.e.
16, R = Me, 52% yield, >95:5 d.r., 96% e.e.

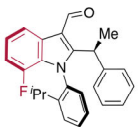

17, 57% yield
>95:5 d.r., 86% e.e.

d Scale-up and late-stage transformations

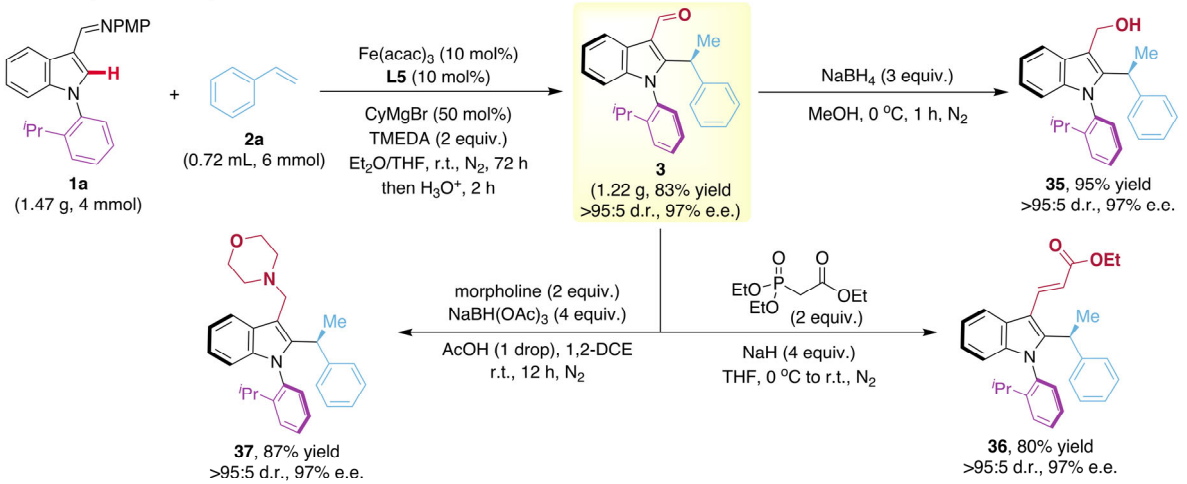

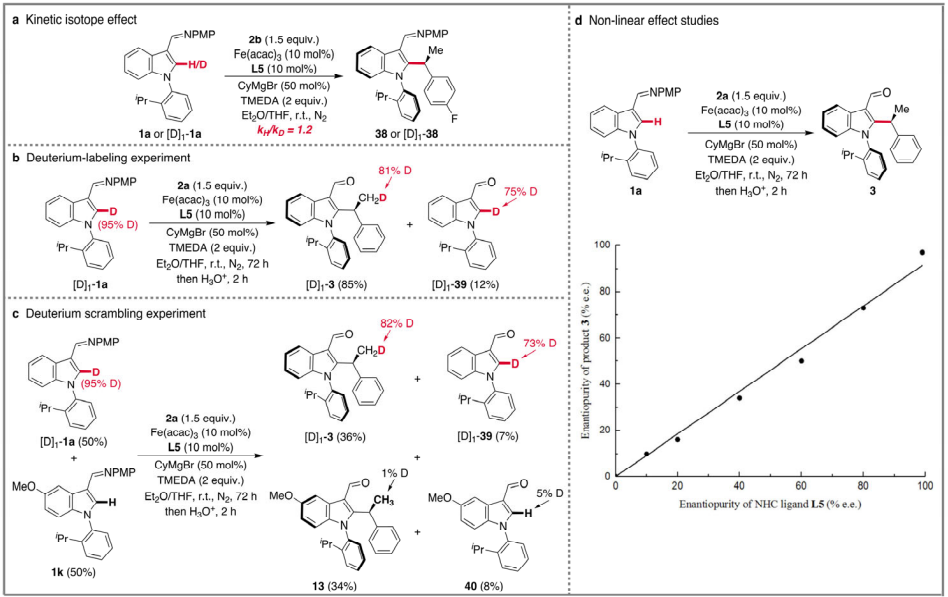
a Kinetic isotope effect
NPMP
H/D
iPr
1a or [D]1-1a
2b (1.5 equiv.)
Fe(acac)3 (10 mol%)
L5 (10 mol%)
CyMgBr (50 mol%)
TMEDA (2 equiv.)
Et2O/THF, r.t., N2
kH/kD = 1.2
Me
F
38 or [D]1-38
b Deuterium-labeling experiment
D
(95% D)
[D]1-1a
2a (1.5 equiv.)
Fe(acac)3 (10 mol%)
L5 (10 mol%)
CyMgBr (50 mol%)
TMEDA (2 equiv.)
Et2O/THF, r.t., N2, 72 h
then H3O+, 2 h
81% D
CH2D
[D]1-3 (65%)
75% D
[D]1-39 (12%)
c Deuterium scrambling experiment
[D]1-1a (50%)
1k (50%)
MeO
2a (1.5 equiv.)
Fe(acac)3 (10 mol%)
L5 (10 mol%)
CyMgBr (50 mol%)
TMEDA (2 equiv.)
Et2O/THF, r.t., N2, 72 h
then H3O+, 2 h
82% D
[D]1-3 (36%)
73% D
[D]1-39 (7%)
1% D
CH3
13 (34%)
5% D
40 (8%)
d Non-linear effect studies
2a (1.5 equiv.)
Fe(acac)3 (10 mol%)
L5 (10 mol%)
CyMgBr (50 mol%)
TMEDA (2 equiv.)
Et2O/THF, r.t., N2, 72 h
then H3O+, 2 h
1a
3
Enantiopurity of product 3 (% e.e.)
Enantiopurity of NHC ligand L5 (% e.e.)
0
20
40
60
80
100

a Synthesis of low-valent iron species

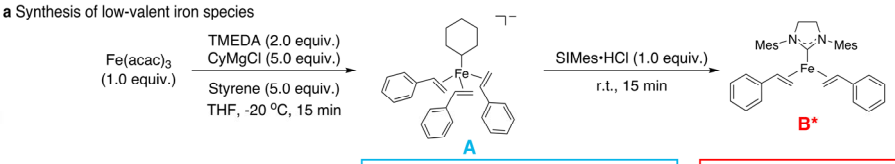

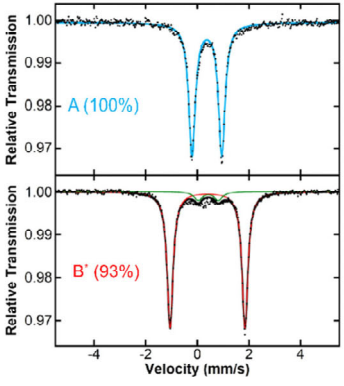

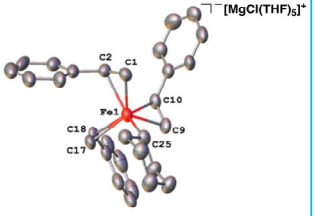

Fe(1)-C(1)	2.062(6)
Fe(1)-C(2)	2.219(6)
Fe(1)-C(17)	2.108(6)
C(1)-Fe(1)-C(25)	93.2(3)
C(2)-Fe(1)-C(25)	127.4(3)
C(1)-Fe(1)-C(2)	37.8(3)
C(1)-Fe(1)-C(9)	118.0(2)
C(1)-Fe(1)-C(10)	98.8(2)
C(2)-Fe(1)-C(9)	125.7(2)
C(2)-Fe(1)-C(10)	90.4(2)

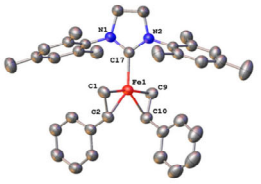

Fe(1)-C(1)	2.046(3)
Fe(1)-C(2)	2.067(2)
Fe(1)-C(17)	2.020(2)
C(1)-Fe(1)-C(2)	40.35(11)
C(1)-Fe(1)-C(9)	171.32(11)
C(1)-Fe(1)-C(10)	131.26(11)
C(2)-Fe(1)-C(10)	91.48(11)
C(9)-Fe(1)-C(2)	131.04(11)
C(1)-Fe(1)-C(17)	95.08(10)
C(2)-Fe(1)-C(17)	135.10(10)

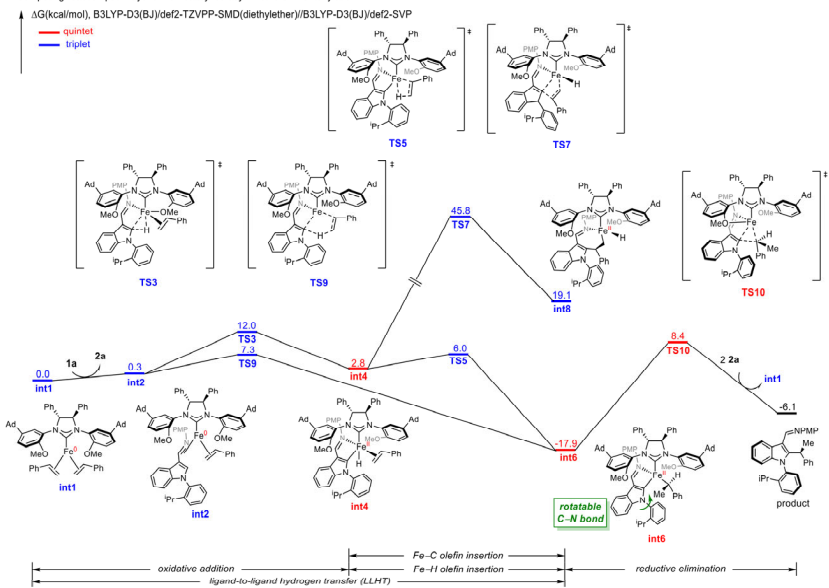
a Competing reaction pathways for iron-catalyzed asymmetric C–H alkenylation
ΔG(kcal/mol), B3LYP-D3(BJ)/def2-TZVPP-SMD(diethylether)//B3LYP-D3(BJ)/def2-SVP
quintet
triplet
TS5
TS7
TS3
TS9
TS10
45.8
TS7
19.1
int8
12.0
TS3
7.3
TS9
0.0
int1
1a
2a
0.3
int2
2.8
int4
6.0
TS5
8.4
TS10
2 2a
int1
-6.1
-17.9
int6
rotatable
C–N bond
product
int1
int2
int4
int6
oxidative addition
Fe–C olefin insertion
Fe–H olefin insertion
reductive elimination
ligand-to-ligand hydrogen transfer (LLHT)

b Optimized structures and relative energies of reductive elimination transition states

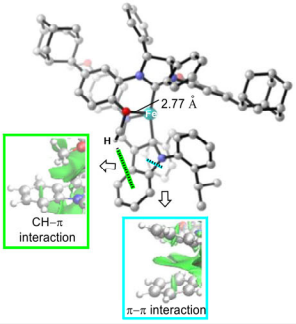

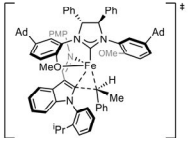

TS10 (R_a,*S*) major product
$\Delta\Delta G^{\ddagger}$ = 0.0 kcal/mol

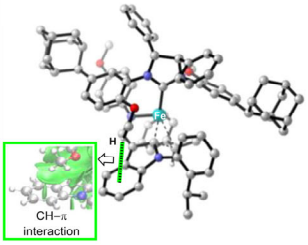

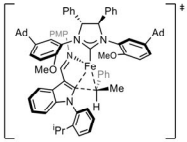

TS10 (R_a,*R*) minor product
$\Delta\Delta G^{\ddagger}$ = 3.5 kcal/mol

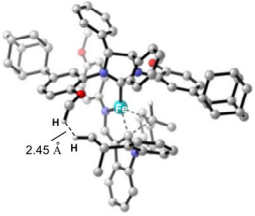

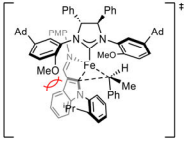

TS10 (S_a,*S*) minor product
$\Delta\Delta G^{\ddagger}$ = 5.1 kcal/mol

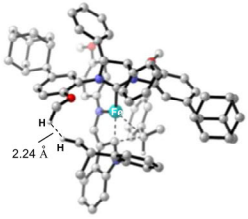

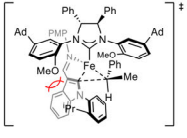

TS10 (S_a,*R*) minor product
$\Delta\Delta G^{\ddagger}$ = 4.5 kcal/mol

b Optimized structures and relative energies of reductive elimination transition states

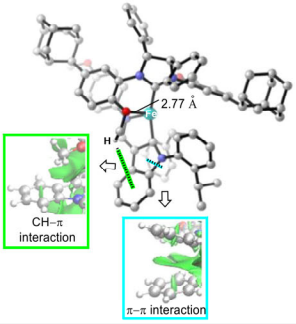

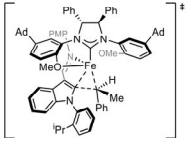

TS10 (R_a,*S*) major product
$\Delta\Delta G^{\ddagger}$ = 0.0 kcal/mol

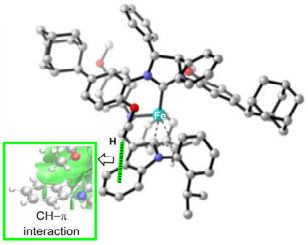

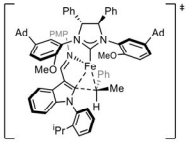

TS10 (R_a,*R*) minor product
$\Delta\Delta G^{\ddagger}$ = 3.5 kcal/mol

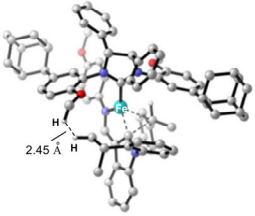

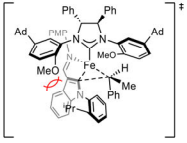

TS10 (S_a,*S*) minor product
$\Delta\Delta G^{\ddagger}$ = 5.1 kcal/mol

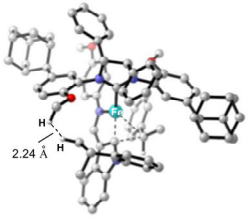

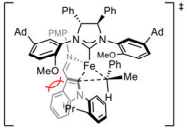

TS10 (S_a,*R*) minor product
$\Delta\Delta G^{\ddagger}$ = 4.5 kcal/mol